iScience

CellPress

Article

Differentiation of Theta Visual Motion from Fourier Motion Requires LC16 and R18C12 Neurons in *Drosophila*

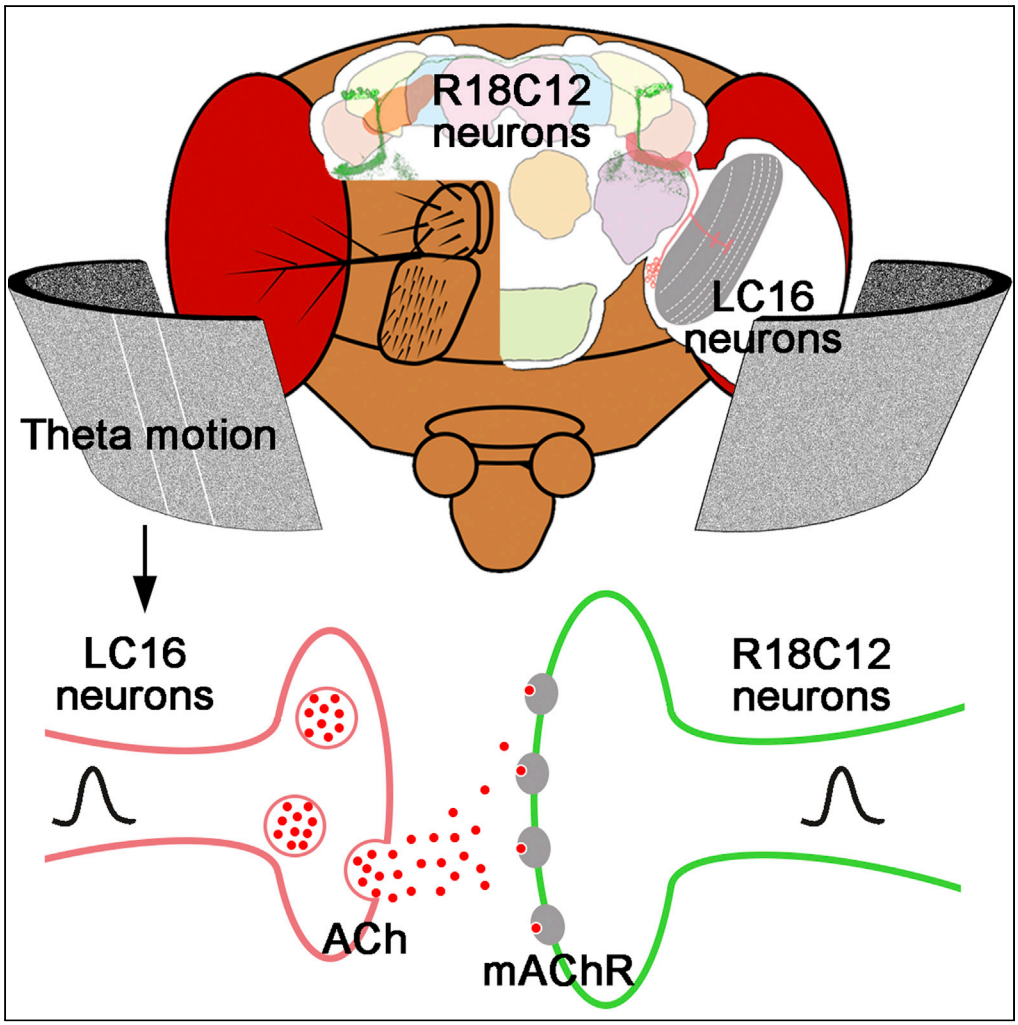

Xiaoxiao Ji, Deliang Yuan, Hongying Wei, ..., Julia Yvonne Gestrich, Li Liu, Yan Zhu

liuli@ibp.ac.cn (L.L.)
zhuyan@ibp.ac.cn (Y.Z.)

HIGHLIGHTS

Perception of theta motion requires LC16 and R18C12 neurons

R18C12 neurons are activated by theta motion

R18C12 neurons form synaptic connections with LC16 neurons

LC16 neurons activate R18C12 neurons through ACh acting on mAChR

Ji et al., iScience *23*, 101041
April 24, 2020
https://doi.org/10.1016/j.isci.2020.101041

iScience

CellPress

Article

Differentiation of Theta Visual Motion from Fourier Motion Requires LC16 and R18C12 Neurons in *Drosophila*

Xiaoxiao Ji,[1,2,4] Deliang Yuan,[1,2,4] Hongying Wei,[1,2,4] Yaxin Cheng,[1,2,4] Xinwei Wang,[1,2] Jihua Yang,[1,2] Pengbo Hu,[1,2] Julia Yvonne Gestrich,[1,2] Li Liu,[1,2,3,5,*] and Yan Zhu[1,2,*]

SUMMARY

Many animals perceive features of higher-order visual motion that are beyond the spatiotemporal correlations of luminance defined in first-order motion. Although the neural mechanisms of first-order motion detection have become understood in recent years, those underlying higher-order motion perception remain unclear. Here, we established a paradigm to assess the detection of theta motion—a type of higher-order motion—in freely walking *Drosophila*. Behavioral screening using this paradigm identified two clusters of neurons in the central brain, designated as R18C12, which were required for perception of theta motion but not for first-order motion. Furthermore, theta motion-activated R18C12 neurons were structurally and functionally located downstream of visual projection neurons in lobula, lobula columnar cells LC16, which activated R18C12 neurons via interactions of acetylcholine (ACh) and muscarinic acetylcholine receptors (mAChRs). The current study provides new insights into LC neurons and the neuronal mechanisms underlying visual information processing in complex natural scenes.

INTRODUCTION

Motion perception is crucial for survival and reproduction in many animals. First-order motion, such as that produced by a brightly colored bird flying through the sky, is defined by spatiotemporal correlations in luminance that obey the theoretical basis of elementary motion detectors (EMDs) (Hassenstein and Reichardt, 1956; Borst and Egelhaaf, 1989). However, the motion of a bird can still be perceived if it flies under the shadow of a leafy tree, even though the coherent space-time correlations in luminance are broken. This type of motion is called higher-order motion, or non-Fourier motion (Chubb and Sperling, 1988; Burr and Thompson, 2011). Widespread in nature, higher-order motion refers to motion containing paradoxical motion cues (Quenzer and Zanker, 1991) or movement of visual objects that have no net motion energy (Chubb and Sperling, 1988; Lee and Nordstrom, 2012). Generally, it is defined by spatiotemporal correlations in signals, including contrast, texture, or various cues other than luminance (Badcock and Derrington, 1985; Cavanagh and Mather, 1989). One type of higher-order motion is theta motion (Zanker, 1990), which contains moving objects with moving textures. Notably, the textures of the objects move coherently in the direction opposite the object movement (Lee and Nordstrom, 2012). The perception of higher-order motion contributes to the discrimination of complex moving features in detailed natural scenes (Aptekar and Frye, 2013). Several studies have reported that, in addition to humans (Lu and Sperling, 1995), higher-order motion can be perceived by fish (Orger et al., 2000) and even flies (Theobald et al., 2008), suggesting convergent evolution for this type of visual perception.

The theoretical model for biological computation of first-order motion was first proposed by Werner Reichardt and Bernard Hassenstein (Hassenstein-Reichardt model of elementary motion) over half a century ago. It has received extensive support from experimental studies of visual systems, including that of fruit flies. However, our understanding of higher-order motion perception is still relatively primitive, without verifiable theoretical models and far fewer publications. Thus, the neural mechanisms underlying higher-order motion perception is an appealing topic.

Ample evidence suggests that first-order and higher-order motion are processed separately, at least in part (Nishida, 2011; Vaina and Cowey, 1996; Vaina et al., 2000). Therefore, how these processes differ and which brain regions are involved need to be further studied. Identifying the responsible neurons in the visual

[1]State Key Laboratory of Brain and Cognitive Science, CAS Center for Excellence in Biomacromolecules, Institute of Biophysics, Chinese Academy of Sciences, 15 Datun Road, Chaoyang District, Beijing 100101, P. R. China

[2]College of Life Sciences, University of the Chinese Academy of Sciences, Beijing 100049, P. R. China

[3]CAS Key Laboratory of Mental Health, Beijing 100101, P. R. China

[4]These authors contributed equally

[5]Lead Contact

*Correspondence: liuli@ibp.ac.cn (L.L.), zhuyan@ibp.ac.cn (Y.Z.)

https://doi.org/10.1016/j.isci.2020.101041

processing pathways is an essential first step. In cats, Y ganglion cells have been found to respond to higher-order motion, implementing demodulating nonlinearity of complex visual features, which indicates a distinct pathway for responses to non-Fourier visual features (Demb et al., 2001; Rosenberg et al., 2010; Rosenberg and Issa, 2011). However, aside from Y ganglion cells, no specific neuronal circuits underlying the perception of higher-order motion have been identified in mammals.

In the visual systems of insects, scientists have identified several types of neurons that respond to higher-order motion, such as T5 neurons and lobula plate tangential cells (Quenzer and Zanker, 1991; Lee and Nordstrom, 2012; Aptekar et al., 2015). The lobular tangential cells LT10 and LT11 are thought to participate in the perception of motion-defined higher-order motion in *Drosophila* (Zhang et al., 2012). Additional behavioral and physiological evidence from studies of flies has also suggested separate processing pathways for first-order elementary motion (EM) and higher-order figure motion (FM) (Aptekar et al., 2012; Lee and Nordstrom, 2012; Theobald et al., 2010; Bahl et al., 2013; Schnell et al., 2012).

Since the discovery that *Drosophila* is able to detect higher-order motion, which had been commonly believed to require a more powerful nervous system, the underlying neural mechanism has been a compelling research subject. One reason is that neither the circuity nor the computational algorithm is clear in fruit flies or in more complex organisms. The hope is that success with the relatively simple nervous system of the fruit fly will lead to a rapid breakthrough that provides clues as to how other animals detect higher-order motion. In recent years, rapid development of experimental methods and techniques for genetic manipulation in the fruit fly has led to substantial progress in identifying the neural circuits underlying first-order motion (Borst and Helmstaedter, 2015; Mauss et al., 2017). The progress and technical advances would also help to understand how an animal, such as a fruit fly, processes complex natural visual scenes beyond relatively simple first-order motion.

The studies on lobula plate have revealed its important roles in first-order motion perception (Borst and Helmstaedter, 2015; Mauss et al., 2017). However, the functions of lobula need to be further investigated. Recently, 22 kinds of visual projection neurons (VPNs) in the lobula have been identified (Wu et al., 2016). These neurons carry retinotopic visual signals from upstream neuropils and project to the central brain where the axon terminals from different VPNs form separate non-retinotopic optic glomeruli. Moreover, previous research has shown that specific VPNs are responsible for specific behaviors. For example, lobula columnar (LC) 6 and LC16 cells sense looming objects (Wu et al., 2016). Additionally, LC16 cells trigger retreat behavior through the moonwalker descending neurons (Sen et al., 2017). A growing body of evidence suggests that the optic glomeruli encode visual information in the same way as olfactory glomeruli (Keleş and Frye, 2017). Activation patterns formed by different combinations of optic glomeruli might be responsible for particular features of visual objects. To answer this question, the specific function of LC neurons and those downstream of them should be investigated. Knowing the function of LC neurons might help to explain the features that are processed in the visual pathway. Except for the giant fiber, other neurons directly downstream of LCs remain unknown (Ache et al., 2019). Searching for neurons directly downstream of LCs and investigating the signal transduction from LCs to the downstream neurons might help clarify the mechanisms underlying the perception of higher-order motion.

In the current study, we developed a paradigm that allowed us to discern first-order and higher-order motion-processing ability in freely walking flies. Using this paradigm, we identified a group of critical neurons in the central brain, namely, R18C12, which were specifically involved in the perception of theta motion. This was accomplished through signals from the lobular visual projection neurons LC16 via mAChRs. Our results indicate a specific neuronal pathway for perceiving higher-order motion and provide support for the idea that first-order and higher-order motion are processed separately.

RESULTS

Tracking Theta Motion in Freely Walking Flies

We developed a simple paradigm that was suitable for large-scale behavior-based screening (Figure 1A). In our paradigm, one single wing-clipped fly was put on a round platform at the bottom of the setup and presented with different visual motion stimuli via a cylindrical LED screen that surrounded them. When flies tracked apparent visual motion, it resulted in circular trajectories that were quantifiable using image analysis (Figures 1B and 1C). We measured the portion of the time a fly spent tracking the motion and designated it as the performance index (PI, Figure 1B, for details see Transparent Methods). The overall tracking

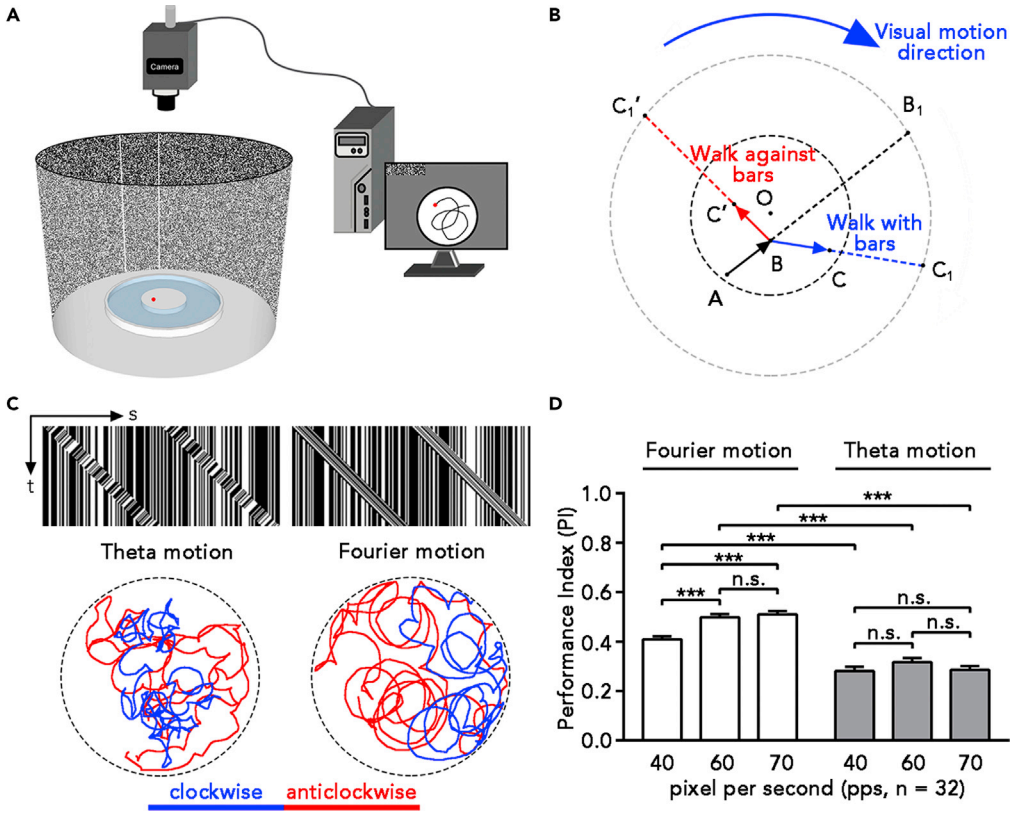

Figure 1. A Paradigm for Evaluating Visual Motion Perception in Freely Walking Flies

(A) A schematic diagram of the experimental apparatus. Red dots represent the wing-clipped flies.

(B) A schematic diagram of trajectory analysis. The black dashed circle indicates the border of the platform. The gray dashed circle indicates the LED screen. The curved blue arrow outside the circle represents the direction of the moving bars in the visual motion stimuli. When a fly walked from A to B to C (or C′) in two sequential frames, projection of its trajectory on the outer circle form point B_1 and C_1 (or C_1′). The direction of the movement from B_1 to C_1 (or C_1′) represented the turning response of the fly to the visual motion. When presented with a clockwise stimulus (blue arrow), we calculated the proportion of time spent walking with the visual motion (A-B-C) or walking against it (A-B-C′). Their difference was used as an indicator of behavioral performance (see details in Transparent Methods).

(C) Space-time plots of theta and Fourier motion stimuli (upper panels). Only a single row of the stimuli is shown here. Changes over time are displayed from top to bottom. For theta motion, the bars moved rightward (the window motion) but the dots inside the bars moved leftward (the contrast motion) at the same speed. Lower panels show the walking trajectories of WTCS flies presented with theta and Fourier motion stimuli. Blue and red lines represented the trajectories corresponding to the clockwise and anticlockwise motion stimuli, respectively.

(D) The PI scores of WTCS flies when presented with theta and Fourier motion stimuli at various speeds (mean + SEM; n = 32 each; n.s., not significant, $p > 0.05$; ***$p < 0.001$; Mann-Whitney test).

See also Figures S1, S2 and S5.

performance was reflected in the average PI toward clockwise-rotating (PI_{clc}) and anticlockwise-rotating ($PI_{anticlc}$, Figures S1A–S1C) stimuli over the test periods (90 s each). In addition to tracking behavior itself, we also calculated locomotion activity, speed, and distance from the flies' movement trajectories (Figures S1D–S1F).

After pilot tests, we used two rotating bars spaced 180° apart on the LED display as the visual stimuli. Wild-type Canton-S (WTCS) flies were able to track both higher-order theta motion and first-order Fourier motion (Figure 1C and Video S1). Over a broad range of speeds for both types of visual motion stimuli, the wild-type flies exhibited strong and consistent tracking responses (Figure 1D). Notably, flies showed weaker responses toward theta motion than to Fourier motion in all tested conditions (Figure 1D). Unlike Fourier motion, in theta motion, the direction that the dotted patterns moved (contrast motion) was opposite that of the visual bar (window motion). Flies exhibited turning behavior when exposed to visual motion

stimuli, including turning with and turning against the motion. To estimate the relative contributions of the two kinds of turns to overall performance, we separated the PIs in Figure 1D into responses for turning with and turning against the visual motion (Figure S1G). When exposed to theta motion stimuli, turning with the motion was turning with the moving bars (window motion), whereas turning against the motion was turning with the patterns inside the bars (first-order motion). As the difference in PI values under Fourier motion and theta motion could also be caused by a difference in the overall time spent walking or in the proportion of time spent turning, we further quantified the amount of time WTCS flies spent walking and the time they walked straight when presented with the visual motion stimuli. As shown in Figures S1H and S1I, the walking activities (the fraction of walking time in a 90-s observation period) and the proportion of straight walks (the fraction of time spent walking relatively straight in the 90 s) were similar for Fourier motion and theta motion and were not influenced by the moving speed of either visual motion.

Because the composition, angular velocity, and angular position of visual motion might affect the visual response, we used high-resolution videos to further analyze the instantaneous response (walking distance and turning angle) of WTCS flies in relation to the movement of visual bars. The main parameters, including the direction of walking (heading) and angle of turning (changes of heading), were calculated every 0.1 s (Figure S2A). The direction and speed of visual motion were derived from a video and used to generate parameters such as the angular position and angular velocity of the motion bars from the point view of the fly. Importantly, we dynamically assigned the two motion bars (180° apart) as the current anterior motion bar and the current posterior motion bar. For this set of analyses, the motion bars always rotated clockwise, and a clockwise rotation or turn defined a positive angle (Figure S2A).

The distribution of heading angles indicated that heading frequencies were similar across all directions (Figures S2B and S2C), confirming the isotropic nature of our setup. At all walking directions, flies turned with the visual motion (turning angle >0°) more than they turned against the visual motion (turning angle <0°). Notably, the tendency to turn with the motion was higher for the Fourier motion condition than for the theta motion condition (Figures S2B and S2C), indicating that flies exhibited weaker tracking responses toward theta motion. This was consistent with the quantification results using PI values in Figure 1D.

The distribution of view angles for the motion bars indicated that, when presented with Fourier motion, flies had a high tendency to keep one moving bar in front of it (Figures S2D–S2F) and the other behind it (Figure S2G). Interestingly, instead of centering at 0°, turning-with-motion events were biased toward the right-front visual field of the flies, centered at about 18° (median: 17.8, the 50% population was between 5.4° and 31.0°) (Figures S2D and S2E). This suggests a strong tracking response toward the anterior motion bar moving clockwise from 0° to 40° (regressive). Furthermore, the distribution of view angles for the posterior motion bar in Figure S2G was broader than that of the anterior bar in Figure S2D, suggesting that the anterior motion bar was more effective, although both bars induced the flies to turn with the visual motion. Together, the PI values toward Fourier motion largely reflect the response of flies to the regressive bar in front of them.

Similar distributions of the view angles and turning angles were observed in WTCS flies when presented with theta motion (Figures S2H–S2K). However, comparing the response to Fourier motion (Figures S2D–S2F) and theta motion (Figures S2H–S2J) revealed a lower response toward theta motion. This was driven by fewer turn-with-motion events in the right-front quadrant (corresponding to frontal regressive motion) and more turn-against-motion events in the left-front quadrant (corresponding to frontal progressive motion) (Figures S2E and S2I). This might have been due to a negative effect of the first-order motion component (the dots rotated anticlockwise to induce an opposite tracking response) of theta motion (the bar rotating clockwise). Other mechanisms unrelated to first-order motion, but inherently related to high-order motion processing, also likely influence the visual behavior.

Like tethered flight in a flight simulator or fixed walking on a suspended ball, our paradigm provides an effective alternative for investigating the neural mechanisms underlying higher-order motion perception.

Identifying Neurons Critical for Perception of Theta Motion but Not Fourier Motion

To identify neurons involved in the perception of theta motion, we performed a behavioral screen using our paradigm. We screened approximately 420 Gal4 lines that were crossed with UAS-TNTE flies to block synaptic transmission in the corresponding Gal4 labeled neurons (Brand and Perrimon, 1993; Sweeney et al.,

1995). Flies with candidate neurons silenced were evaluated for their response to theta motion. We identified three Gal4 lines with defective responses, R18C12-, R15D05-, and R25E04-Gal4. When Gal4-labeled neurons in these lines were blocked by tetanus toxin light chain, flies exhibited significantly decreased responses toward theta motion but normal responses to Fourier motion (Figure 2A). Among the three silenced lines, R18C12>TNTE and R15D05>TNTE flies did not show any signs of locomotion difficulty, including moving activity, speed, and distance (Figure S3). Blocking a majority of Gal4-labeled neurons did not cause significant deficits in perceiving theta motion. Four examples are shown in Figure S4A, highlighting the specific roles of R18C12 neurons in theta motion detection.

To confirm that silencing the neurons labeled by the three Gal4s results in defective perception of theta motion, we silenced these neurons with Kir2.1, an inwardly rectifying potassium channel that causes membrane hyperpolarization (Baines et al., 2001). Both R18C12>Kir2.1 flies and R15D05>Kir2.1 flies showed significantly decreased responses to theta motion but responded normally to Fourier motion (Figures S4B and S4C). The R25E04>Kir2.1 flies were embryonic lethal.

To identify which neurons were involved in theta motion perception circuits, we examined the expression pattern of the three Gal4s using UAS-mCD8::GFP. Confocal imaging revealed that these Gal4s contained the same two clusters of neurons (Figures S4D–S4Fii). Considering the expression pattern of the Gal4s and the motor abilities in these blocked flies, we chose R18C12-Gal4 for the subsequent experiments that investigated the cellular mechanisms underlying theta motion perception. The R18C12-Gal4-labeled neurons were named R18C12 neurons.

To determine whether R18C12 neurons are also involved in the perception of other types of higher-order motion, we exposed flies to theta-like (TL) motion and drift-balanced (DB) motion and their corresponding first-order motions, Fourier motion TL and Fourier motion DB (Figures S5A and S5B, Videos S2 and S3). WTCS flies were able to track theta-like motion, drift-balanced motion, and the corresponding first-order motions (Figures S5A and S5B). Perception of theta-like motion in the R18C12>TNTE or R18C12>Kir2.1 flies was significantly decreased, compared with the genetic controls (Figures S5C and S5E). Notably, flies with silenced R18C12 neurons responded normally to drift-balanced motion and Fourier motion DB, suggesting that R18C12 neurons are not required for the perception of drift-balanced motion or that redundant sensing pathways might exist (Figures S5D and S5F).

The results showed that inactivating the R18C12 neurons led to a significant reduction in perception of theta and theta-like motion, without compromising the ability to perceive first-order motion. Therefore, R18C12 neurons are required for the perception of at least two types of high-order motion.

R18C12 Neurons Are Located in an Important Visual Processing Center

R18C12-Gal4 mainly labeled two clusters of neurons, one on each side of the brain (Figures 2B and 2C). These neurons innervated the ventrolateral protocerebrum (VLP), which is considered to be involved in visual processing (Ito et al., 2014). The two clusters of neurons were symmetrical and possibly interconnected with each other through the nerve fibers above the superior medial protocerebrum (SMP) (Figures 2C and 2D, hollow triangle). The cell bodies of R18C12 neurons were located between the superior intermediate protocerebrum (SIP) and the lateral horn (LH), in front of the anterior superior lateral protocerebrum (SLP) and above the anterior optic tubercle (AOTU) (Figures 2C and 2D, arrowhead). Counting the number of nuclei in R18C12>nlsGFP flies revealed a total of 16.96 $\pm$ 2.293 (mean $\pm$ SD, n = 24) labeled cells in one cluster (Figure 2E). We found no significant differences in the number of labeled cells between male and female flies, or between the left and right hemisphere.

Most nerve fibers of R18C12 neurons were bundled together and projected to the dorsal posterior VLP where they formed a dense structure with widespread tree-like dendrites that innervated the dorsal VLP. In addition, several fibers projected to the medial dorsal VLP to form a relatively low-density structure compared with the structure described above (Figure 2C, arrow). In addition to the VLP, R18C12-Gal4 also weakly labeled the AOTU. Notably, R18C12-Gal4 did not label any visual neurons in the optic lobe, suggesting that the impaired perception of higher-order motion in flies when blocking R18C12 neurons was unlikely to be caused by dysfunctions of the optic lobes (Figures S4D–S4Fii).

To analyze the input and output sites of R18C12 neurons, we expressed green fluorescent protein (GFP)-fused synaptotagmin (Syt) (Zhang et al., 2002; Christiansen et al., 2011) and nAChR-Dα7 (Dα7) (Leiss

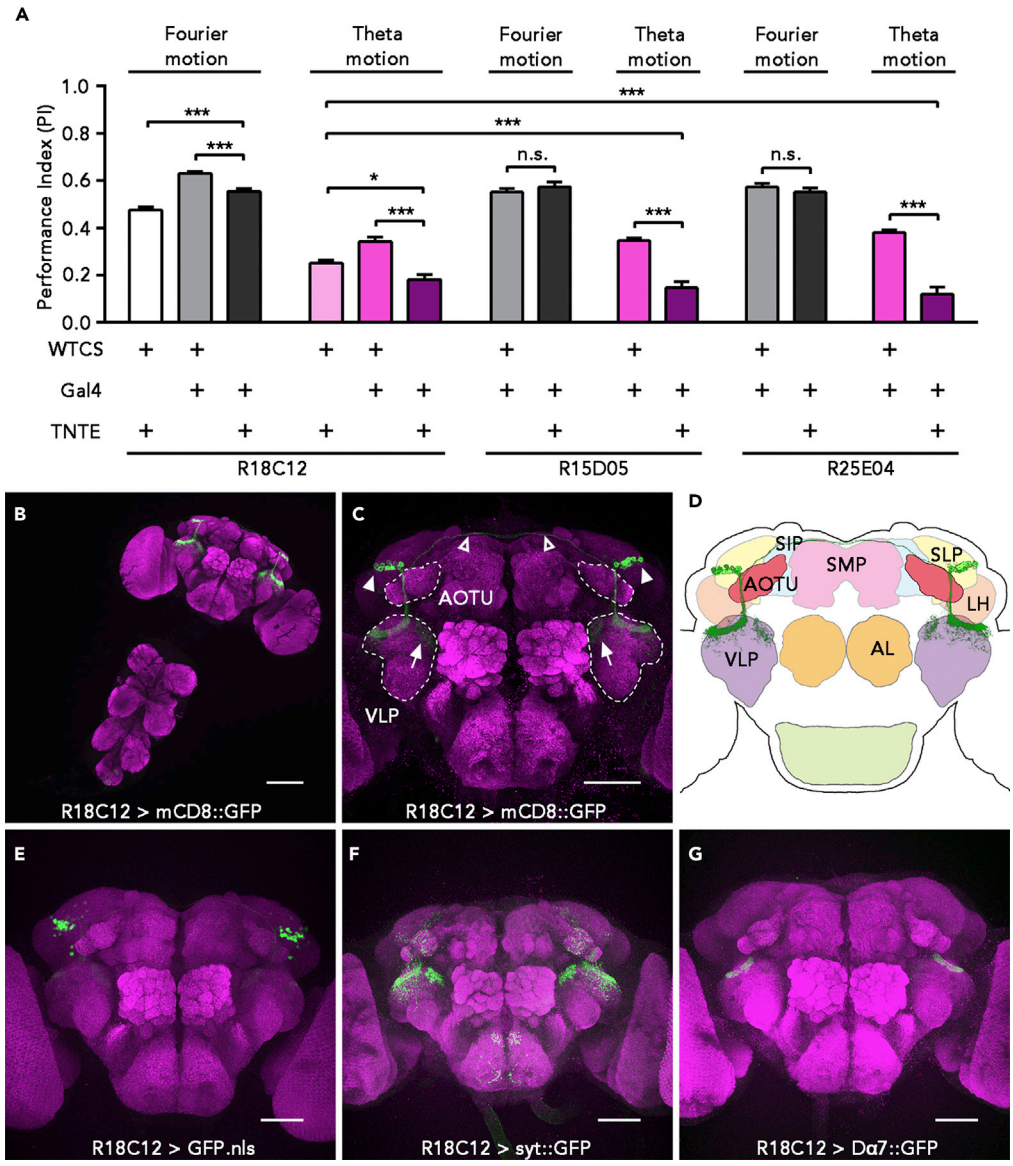

Figure 2. R18C12 Neurons Were Specifically Involved in Perception of Theta Motion

(A) The performance indexes (PIs) of R18C12>TNTE, R15D05>TNTE, R25E04>TNTE flies and their genetic controls when presented with Fourier motion and theta motion stimuli at 60 pps. Black and gray bars indicate the responses to Fourier motion, whereas light and dark purple bars indicate the responses to theta motion (mean + SEM; n = 20–32; n.s., not significant, $p > 0.05$; *$p < 0.05$; ***$p < 0.001$; Mann-Whitney test).

(B) Expression pattern of mCD8::GFP under the control of R18C12-GAL4 in the central brain and VNC. Scale bar, 100 μm.

(C) Expression pattern of R18C12>mCD8::GFP in the central brain.

(D) A schematic diagram referring to the morphology and location of R18C12 neurons (green).

(E) Cell bodies of R18C12 neurons labeled by nuclear GFP.

(F) Presynaptic region of R18C12 neurons labeled by UAS-syt::GFP.

(G) Postsynaptic region of R18C12 neurons marked by UAS-Dα7::GFP.

Scale bar applied to (C) and (E–G), 50 μm. SMP, superior medial protocerebrum; SIP, superior intermediate protocerebrum; SLP, superior lateral protocerebrum; AOTU, anterior optic tubercle; VLP, ventrolateral protocerebrum; LH, lateral horn; AL, antennal lobe; GFP signals are shown in green, and nc82 signals (as counterstain) are shown in magenta. See also Figures S3–S5.

et al., 2009) in R18C12 neurons to visualize the pre- and post-synaptic regions, respectively. The distribution of Syt::GFP signals was similar to mCD8::GFP, except for strong signals in the VLP branches and faint signals in regions of cell bodies (Figure 2F). R18C12>Dα7::GFP primarily labeled a restricted region inside of the dense structure at the top of the posterior VLP (Figure 2G). These results indicate that R18C12 neurons receive most information from the dorsal posterior VLP and send information out over a broader range of sites, including the dorsal VLP and AOTU.

In summary, R18C12-Gal4 labeled two symmetrical clusters of neurons that innervated the VLP, suggesting that R18C12 neurons are directly involved in visual information processing of VLP on signals from the optic lobes.

R18C12 Neurons Are Activated Specifically by Theta Motion

To examine how R18C12 neurons respond to theta motion stimuli, we performed patch-clamp recordings on GFP-labeled R18C12 neurons while presenting the visual motion to the flies (Figure 3A). When presented with a theta motion stimulus, R18C12 neurons showed strong depolarization (Figure 3B, right). In contrast, applying a Fourier motion stimulus resulted in a weak and delayed response, which might have been an under-threshold response that could not elicit spikes (Figure 3B, left). To quantify the R18C12 neuronal responses to both types of visual motion stimuli, we calculated the maximum action potential frequencies using Spikes 2.0 software (Figure 3C) and found that theta motion stimuli induced significantly stronger responses than Fourier motion stimuli, which suggested that R18C12 neurons were specifically responsible for processing theta motion.

We next used the calcium sensor calcium-modulated photoactivatable ratiometric integrator (CaMPARI) to visualize the response of R18C12 neurons to theta motion at the population level (Fosque et al., 2015). As shown in Figures 3D–3Dii, when flies were presented with a theta motion stimulus, the CaMPARI signals in R18C12 neurons were photo-converted from green to red in the presence of 405-nm light. In contrast, no color changes occurred in the flies presented with static dots (control) (Figures 3E–3Eii). Importantly, photo-conversion of the R18C12 neurons did not occur when flies were presented with Fourier motion (Figures 3G–3Hii). To quantify the activity of R18C12 neurons, we calculated the relative ratio of red versus green fluorescent signals in the cell bodies of R18C12 neurons and found that these ratios also indicated a significantly stronger response to theta motion than to Fourier motion (Figures 3F and 3I).

Together, these results strongly support the hypothesis that R18C12 neurons are responsible for processing theta motion but not Fourier motion.

R18C12 Neurons Form Synaptic Connections with LC16 Visual Projection Neurons

The pre- and post-synaptic sites of the R18C12 neurons indicated that potential upstream and downstream neurons should innervate the top region of the VLP. We analyzed the known expression patterns of different Gal4s and found that LC16 visual projection neurons had targeting sites in optic glomeruli that potentially overlapped with the post-synaptic sites of R18C12 neurons (Figures 4A, S6A and S6B). Moreover, analyzing the pre- and post-synaptic regions of LC16 neurons suggested that they might exchange information with R18C12 neurons through this overlapping region (Figures 4B and 4C).

To determine whether LC16 neurons form direct connections with R18C12 neurons, we performed GFP reconstitution across synaptic partners (GRASP) (Gordon and Scott, 2009) and target GRASP (t-GRASP) (Shearin et al., 2018) experiments. The GRASP signals of reconstituted GFP were distributed in the top VLP region, suggesting the dendrites of R18C12 neurons and LC16 neurons were located in close proximity to each other (Figure S6C). Importantly, we observed t-GRASP signals when testing whether the LC16 neurons were upstream of the R18C12 neurons (Figure 4D) but not when testing if they were downstream (Figure S6D). To determine whether LC16 neurons participate in theta motion perception, we blocked LC16 neurons using OL0092C-Gal4 as the driver and presented the flies with theta and Fourier motion. Both OL0092C>TNTE and OL0092C>Kir2.1 flies exhibited severely reduced perception of theta motion but relatively normal perception of Fourier motion (Figures 4E and S6E). Therefore, LC16 and R18C12 neurons might act as upstream-downstream partners in processing theta motion information.

We next investigated whether these neurons formed functional synapses by measuring changes in R18C12 activity while artificially stimulating the upstream LC16 neurons (Figure 4F). For this purpose, we generated

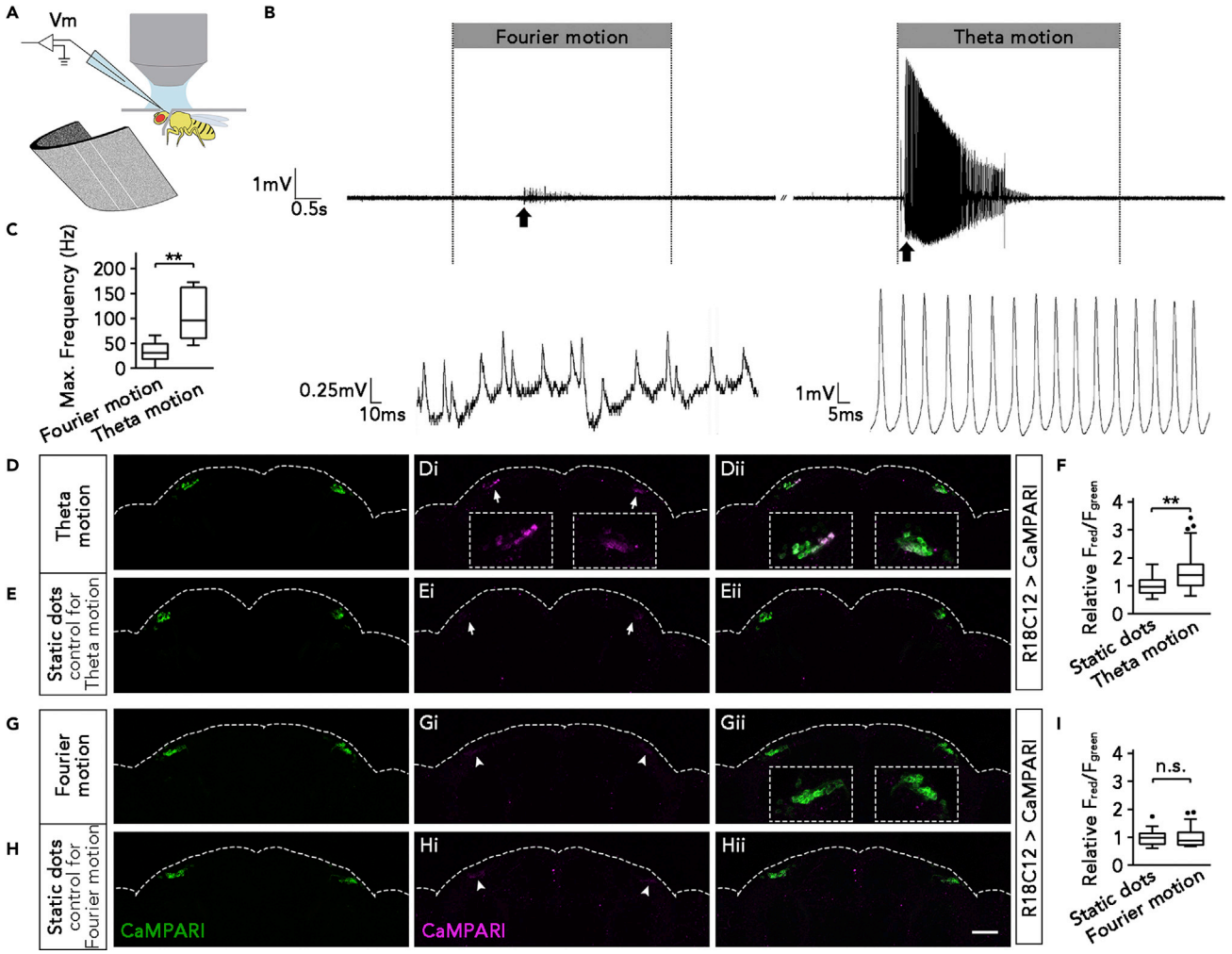

Figure 3. R18C12 Neurons Were Activated by Theta Motion

(A) Schematic diagram of electrophysiological experiments showing the fly holder, the recording electrode, and the display for presenting stimuli.

(B) Representative results of *in vivo* patch-clamp recordings from R18C12 neurons stimulated with clockwise Fourier motion (left) and theta motion (right). The recording trace showed a phasic-tonic response to the theta motion stimulus. Detailed recording traces are shown at expanded time scales below.

(C) Maximum firing rates for the Fourier and theta motion groups (n = 8; **p < 0.01; paired t test). The maximum spike rate (Max Frequency) was the largest response rate for the neuron and was calculated by Spikes 2.0 software.

(D and E) Visualization of active neurons in response to visual motion using CaMPARI (the arrows indicate the position of R18C12 cell bodies). (D–Dii) The green CaMPARI (D) in the R18C12 neurons photoconverted to red (Di) in some R18C12 neurons when flies were presented with theta motion stimuli. (Dii) The merged image of (D) and (Di). The dotted boxes on the bottom show the magnified region of cell bodies pointed to by the arrows. (E–Eii) Photo-conversion of the R18C12 neurons did not occur when static dots were used instead of theta motion as a control.

(F) Quantitation of the relative red/green CaMPARI fluorescence in R18C12 neurons stimulated by either theta motion or static dots (control) (n = 42; **p < 0.01; Wilcoxon matched-pairs signed rank test).

(G–I) R18C12 neurons were not activated by Fourier motion. (G and H) The green CaMPARI in the R18C12 neurons was not photoconverted to red (the arrow heads indicate the position of R18C12 cell bodies) when flies were presented with Fourier motion stimuli (Gi and Gii) or static dots (Hi and Hii). Scale bar, 50 μm. (I) Quantitation of the relative red/green CaMPARI fluorescence in R18C12 neurons stimulated by either Fourier motion or static dots (n = 19; n.s., not significant, p > 0.05; paired t test). Boxplots indicate the median and middle 50% of the data, while Tukey whiskers are used to indicate variability outside the upper and lower quartiles.

a fly strain that expressed P2X2 channels (ATP-gated cation channels; Lima and Miesenböck, 2005) in the LC16 neurons and GCaMP6s (a calcium indicator) in the R18C12 neurons. In the experimental group, R18C12 neuronal activity increased significantly after stimulating LC16 neurons with 1 mM ATP (Figure 4G). In contrast, R18C12 neurons in the control flies were only activated by the application of 20 mM KCl, suggesting that these neurons were viable but did not directly respond to ATP (Figures 4H and 4I).

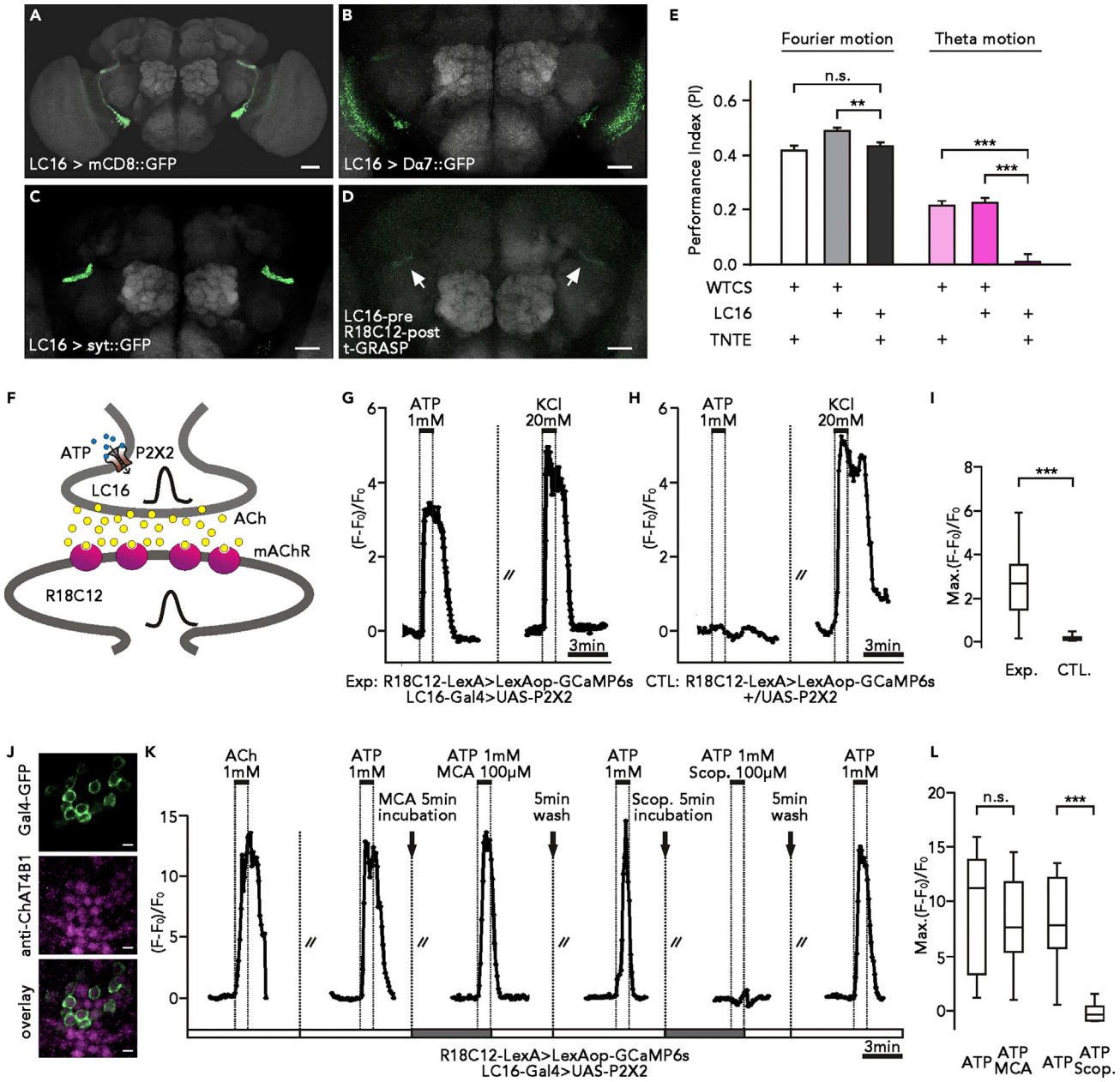

Figure 4. LC16 Neurons Act Upstream in Theta Motion Perception, Releasing ACh onto R18C12 Neurons through mAChRs

(A) Expression of mCD8::GFP under the control of LC16-GAL4 (OL0092C) in the central brain.

(B) Postsynaptic region of LC16 neurons marked by UAS-Dα7::GFP.

(C) Presynaptic region of LC16 neurons labeled by UAS-syt::GFP.

(D) The t-GRASP signal (green, indicated by arrows) reconstituted by post-t-GRASP (GFP1-10) under the control of R18C12-LexA and pre-t-GRASP (GFP11) under the control of LC16-Gal4 (OL0092C). Nc82 (gray) served as counterstaining. Scale bar applied to (A)–(D), 30 μm.

(E) The performance index values for LC16>TNTE flies and their genetic controls when presented with Fourier motion and theta motion stimuli at 60 pps (mean + SEM; n = 20 each; n.s., not significant, $p > 0.05$; **$p < 0.01$; ***$p < 0.001$; unpaired t test).

(F) Schematic diagram of the experimental design for testing the connection between LC16 and R18C12 neurons via functional imaging.

(G–I) Changes in activity in R18C12 neurons after stimulating LC16 neurons. (G) Experimental groups (Exp) showed increased activity after treatment with 1 mM ATP or 20 mM KCl. (H) The control groups (CTL) showed no ATP-related response. (I) Significant differences of $\Delta F/F$ in LC16 neurons of Exp and CTL groups (n = 15; ***$p < 0.001$; Kolmogorov-Smirnov test).

(J) Immunostaining of R18C12 neurons with cholinergic markers. (Top) GFP-labeled R18C12 neurons (green), (middle) anti-ChAT4B1 signals (magenta), (bottom) colocalization of both. Scale bar, 2 μm.

Figure 4. *Continued*

(K and L) Activity changes in R18C12 neurons when simultaneously applying different ACh antagonists and activating LC16 neurons with ATP. (K) In calcium imaging experiments, ATP responses were blocked via pre-incubation (5 min) with the muscarinic ACh receptor antagonist scopolamine (Scop, 100 μM) but not with the nicotinic ACh receptor antagonist mecamylamine (MCA, 100 μM). Solid bars at X axis indicated the duration of incubation with antagonists. (L) Increased $\Delta F/F$ in R18C12 neurons in response to ATP-activated LC16 neurons was significantly blocked after Scop treatment (n = 19; ***$p < 0.001$; Wilcoxon matched-pairs signed rank test) but not affected by MCA treatment (n = 19; n.s., not significant, $p > 0.05$; paired t test). Boxplots indicate the median and middle 50% of the data, while Tukey whiskers are used to indicate variability outside the upper and lower quartiles.
See also Figures S6 and S7.

Additionally, ATP increased intracellular Ca^{2+} levels in R18C12 neurons in a dose-dependent manner (500 μM–5 mM), with desensitization occurring at 10 mM (Figure S7A).

Taken together, the structural proximity, synaptic connectivity, and functional causality between the LC16 and R18C12 neurons strongly suggested that R18C12 neurons are a postsynaptic target for LC16 neurons in processing theta motion signals.

Muscarinic Acetylcholine Receptors Mediate Communication at the LC16 to R18C12 Synapses

Because LC16 neurons act as upstream partners of R18C12 neurons, we next surveyed the neurotransmitters involved in the LC16 to R18C12 neuronal signaling. Application of 1 mM ACh effectively elevated intracellular Ca^{2+} levels in R18C12 neurons (Figure S7B), whereas application of other neurotransmitters at 1 mM, including GABA, glutamate, dopamine, octopamine, serotonin, and histamine, had no effect of calcium levels (Figure S7B). To further confirm that the LC16 neurons are indeed cholinergic neurons, we used immunostaining to locate choline acetyltransferase, an enzyme critical for ACh synthesis. As shown in Figure 4J, anti-ChAT4B1 signals colocalized with the GFP-labeled LC16 neurons, suggesting that LC16 neurons could use ACh as neurotransmitter for the signal transduction.

To identify which type of ACh receptor is expressed by R18C12 neurons (muscarinic or nicotinic), we tested different antagonists for their abilities to block the LC16-induced activation of R18C12 neurons. We applied scopolamine (Scop, an mAChR antagonist) or mecamylamine (MCA, a nicotinic AChR antagonist) to the bath 5 min before ATP application. Pre-incubation with scopolamine blocked the ATP-induced Ca^{2+} increase in R18C12 neurons, whereas mecamylamine did not (Figures 4K and 4L). Additionally, the ACh response was not blocked by pre-incubation with 1 μM tetrodotoxin (TTX), ruling out the involvement of other neurons in this process (Figure S7A). Together, these results suggested that R18C12 neurons were activated by LC16 neurons via mAChRs.

DISCUSSION

In the natural environment, animals need to process a large amount of visual information, including higher-order motion. In the current study, we established a paradigm to effectively evaluate the ability of freely walking flies to perceive Fourier (first-order) and theta (higher-order) motion. Through behavioral screening, we identified R18C12 neurons in the central brain as a pivotal component of the neural circuit underlying the perception of theta motion. Furthermore, structural and functional analysis revealed that R18C12 neurons are connected with upstream LC16 visual projection neurons, which likewise play an essential role in theta motion perception. Our study provides the neuronal evidence for critical players in higher-order motion perception both in the optic lobe and in the central brain.

Most optomotor investigations in *Drosophila* have used two classes of behavioral paradigms: tethered flights in a flight simulator (Götz, 1964; Heisenberg and Wolf, 1984; Wolf and Heisenberg, 1980) or fixed walking on an air-suspended ball (Götz and Wenking, 1973). Although freely walking flies have been found to track gratings presented on a cylindrical LED screen in an inherent closed-loop fashion, only a few experiments have investigated responses to visual motion in freely walking flies (Strauss et al., 1997; Katsov and Clandinin, 2008). The amount of work needed to quantitatively evaluate the behavior of hundreds of lines in a reasonable period of time is daunting if one uses the common flight simulator. Instead, we developed a walking paradigm, which enabled us to conduct an effective screen in a reasonable amount of time. Importantly, testing walking flies bypass the requirement for the ability or motivation to fly, overcoming the challenge posed by flies failing to fly after genetic manipulations, which we have commonly faced. Furthermore, in a walking paradigm, the pretreatments and experimental procedures are much simpler, making it

easier to carry out large-scale behavior-based screens. Compared with a flight simulator system, our tracking system is able to calculate the turning direction of the flies at every recording time point. Therefore, it exhibits sufficient resolving power to accurately assess the visual ability of the flies. From the screen, we identified R18C12 cells, which provides a long-sought-after handle for us to peek into the neural circuit and mechanisms of theta motion detection.

What are the roles of LC16 and R18C12 neurons in the visual pathways of *Drosophila*? Our results showed that R18C12 acted as a downstream partner of LC16 to further process theta motion signals. However, blocking LC16 neurons elicited more severe defects in theta motion perception than did blocking R18C12 neurons. This indicated that LC16 plays a crucial role in perceiving theta motion and might relay theta motion signals to neurons other than R18C12 neurons. Moreover, R18C12 neurons might also receive signals from other upstream neurons. When analyzing the morphology of R18C12 neurons and other visual projection neurons, we found that LT10/11 and other LC neurons, such as LC6, LC9, and LC25, might form synapses with R18C12 neurons. The optic glomeruli innervated by visual projection neurons have been suggested to provide parallel pathways to different classes of information (Wu et al., 2016; Keleş and Frye, 2017). Thus, R18C12 neurons might innervate several optic glomeruli that responded to theta motion and other higher-order motion. This was supported by our results that R18C12 neurons were also involved in the perception of theta-like motion (Figure S5). Notably, nerve fibers of R18C12 neurons projected across the midline and connected the two symmetrical clusters of neurons on each side, suggesting communication between the two hemispheres during motion processing. We hypothesize that R18C12 neurons do not simply relay the upstream signals from LC16, but that they also receive visual information from other visual projection neurons in the ipsilateral or contralateral hemispheres. This would allow further processing of theta motion or even other kinds of higher-order motions.

Aside from the pathways involving R18C12 neurons, additional pathways and neurons might also contribute to the perception of theta motion. Indeed, when silencing the R18C12 neurons, the optomotor response to theta motion decreased but was not completely abolished. Although this could be due to incomplete blocking, five types of visual projection neurons, LT10, LT11, LC9, LC10a, and LC12, have also been reported to respond to theta motion (Aptekar et al., 2015; Zhang et al., 2012). These neurons project to different regions of the VLP or the optic tubercle. Our results regarding the LC16-R18C12 pathway do not exclude the possibility that other neurons downstream of LC16 also receive theta motion signals from LC16 or other visual projection neurons. Our silencing screen with TNT also revealed the involvement of neurons other than R18C12 in the perception of higher-order motion. In this screen, 17 of 420 Gal4 lines exhibited reduced tracking ability in response to theta motion. Among these, 13 silenced lines (including R18C12) showed decreased PIs that were significantly higher than zero, three silenced lines showed PIs close to zero, and one silenced line had a negative PI score. Further characterization of those candidates could help build a complete picture of how theta motion is extracted and relayed into the central brain.

To transmit neuronal signals, ACh interacts with two classes of acetylcholine receptors: nicotinic acetylcholine receptors (nAChRs) that are coupled with cation permeable ion channels and muscarinic acetylcholine receptors (mAChRs) that are coupled with G-proteins. In *Drosophila*, nAChRs mediate fast synaptic transmission in the central nervous system. The nAChRs in Tm2 and lobula plate tangential cells (LPTCs) are crucial for motion detection (Brotz and Borst, 1996; Takemura et al., 2011). Recently, an inhibitory mAChR was found to contribute to OFF selectivity in the *Drosophila* larval visual system (Qin et al., 2019). However, little is known about the physiological function of mAChRs in the visual processing of adult flies. Our result that excitatory mAChRs mediated the LC16-R18C12 circuit is intriguing, as nAChRs are more common in the *Drosophila* visual system. We propose that mAChRs play essential roles in high-order motion processing in *Drosophila*, similar to their counterparts in the vertebrate visual system. Vertebrate mAChRs in the primary visual cortex (V1) improve visual perception by regulating neuronal sensitivity via altering membrane conductance, synaptic strength, or connectivity with other neurons (Groleau et al., 2015). Similarly, the post-synaptic mAChRs in R18C12 neurons might broadly influence the connections between R18C12 and other neurons. Another function of mAChRs in V1 is to modulate neuronal synchronization to form macroscopic oscillations that change cortical activity (Groleau et al., 2015; Kang et al., 2014). If this is applicable to flies, the mAChRs in R18C12 might be involved in synchronizing the activities of different neurons related to higher-order motion. Moreover, mAChRs in V1 also contribute to attentional mechanisms (Herrero et al., 2008; Klinkenberg and Blokland, 2010), which seems

to be in accord with the need for theta motion perception in flies. Taken together, mAChRs in R18C12 neurons might not only transmit signals related to theta motion but might also modulate the status of R18C12 neurons and even the local neural network.

Being a functional component involved in theta motion detection, R18C12 cells in the central brain also put the relationship between first-order motion detection and higher-order motion detection into perspective. Photoreceptors serve as the common input for perception of both types of motion. However, although blocking LC16 and R18C12 neurons strongly decreased the perception of theta motion, effects on the perception of first-order motion were minimal, suggesting the neural pathways for processing these types of motion are segregated into distinct streams early in the lobular lobes. Interestingly, other known neurons potentially related to R18C12 in functions located in the peripheral or the optic lobes, including the Y-ganglion cells in cats (Demb et al., 2001; Rosenberg et al., 2010; Rosenberg and Issa, 2011) and the figure-ground discriminating neurons in *Drosophila* (Aptekar et al., 2015). Identifying the R18C12 neurons promise new insights into the signal processing further in the central. Our findings should serve as a reference for further research on higher-order motion both in fruit flies and more complex animals. The next stage of investigation would be to retrogradely survey the upstream neurons to understand where the segregation first occurs.

Limitations of the Study

We demonstrated that R18C12 neurons in the central brain function downstream of LC16 neurons in the pathway that processes theta motion signals. However, the lack of direct recordings from LC16 makes it difficult to distinguish the roles of R18C12 and LC16 neurons in the perception to theta motion. Electrophysiological recordings from these neurons would be ideal for exploring their dynamic properties, but we were unable to do so for two technical reasons. First, unlike R18C12 neurons, LC16 neurons reside deep in the brain. Moreover, operations to prepare the brain for electrophysiological recordings, particularly removing tissue above the LC16 neurons, would likely damage their connections. Second, LC16 neurons represent a large population with small cell bodies, which are unsuitable for direct recording. Because it was challenging to survey all R18C12 neurons, we cannot exclude the possibility that they are functionally homogeneous. Nevertheless, we achieved patch-clamp recordings from several R18C12 neurons, which revealed explicit responses to different visual motions and shed light on neuronal pathways.

METHODS

All methods can be found in the accompanying Transparent Methods supplemental file.

DATA AND CODE AVAILABILITY

The data that support the findings of this study are available from the authors upon reasonable request.

SUPPLEMENTAL INFORMATION

Supplemental Information can be found online at https://doi.org/10.1016/j.isci.2020.101041.

ACKNOWLEDGMENTS

This work was supported by grants from the National Natural Sciences Foundation of China (31871046, 91632107, 91232720, 91632112 and 31800867), the Chinese Academy of Sciences (XDB02040002, QYZDY-SSW-SMC015), and the Ministry of Science and Technology of China (2012CB825504). We thank Dr. Michael Reiser and Dr. Yijin Wang for providing the flies. We thank Haiyun Gong, Yanqiong Zhou, Yifei Du, Shan Gao, and Xudong Zhao of the IBP core facility center for technical assistance. We also thank the Janelia Fly Light Project Team, Bloomington *Drosophila* Stock Centers, and *Drosophila* Genetic Resource Center at Kyoto Institute of Technology.

AUTHOR CONTRIBUTIONS

X.J., H.W., L.L., and Y.Z. designed the study. X.J., D.Y., and Y.C. performed behavioral experiments. X.J. performed CaMPARI and immunostaining experiments. H.W., X.W., J.Y.G., J.Y., and P.H. performed calcium imaging and electrophysiological experiments. X.J., H.W., L.L., and Y.Z. analyzed data and wrote the paper with the help of all authors.

DECLARATION OF INTERESTS

The authors declare no competing interests.

Received: November 12, 2019
Revised: March 9, 2020
Accepted: April 1, 2020
Published: April 24, 2020

REFERENCES

Ache, J.M., Polsky, J., Alghailani, S., Parekh, R., Breads, P., Peek, M.Y., Bock, D.D., von Reyn, C.R., and Card, G.M. (2019). Neural basis for looming size and velocity encoding in the *Drosophila* giant fiber escape pathway. Curr. Biol. *29*, 1073–1081.

Aptekar, J.W., and Frye, M.A. (2013). Higher-order figure discrimination in fly and human vision. Curr. Biol. *23*, R694–R700.

Aptekar, J.W., Keles, M.F., Lu, P.M., Zolotova, N.M., and Frye, M.A. (2015). Neurons forming optic glomeruli compute figure-ground discriminations in *Drosophila*. J. Neurosci. *35*, 7587–7599.

Aptekar, J.W., Shoemaker, P.A., and Frye, M.A. (2012). Figure tracking by flies is supported by parallel visual streams. Curr. Biol. *22*, 482–487.

Badcock, D.R., and Derrington, A.M. (1985). Detecting the displacement of periodic patterns. Vision Res. *25*, 1253–1258.

Bahl, A., Ammer, G., Schilling, T., and Borst, A. (2013). Object tracking in motion-blind flies. Nat. Neurosci. *16*, 730–738.

Baines, R.A., Uhler, J.P., Thompson, A., Sweeney, S.T., and Bate, M. (2001). Altered electrical properties in *Drosophila* neurons developing without synaptic transmission. J. Neurosci. *21*, 1523–1531.

Borst, A., and Egelhaaf, M. (1989). Principles of visual motion detection. Trends Neurosci. *12*, 297–306.

Borst, A., and Helmstaedter, M. (2015). Common circuit design in fly and mammalian motion vision. Nat. Neurosci. *18*, 1067–1076.

Brand, A.H., and Perrimon, N. (1993). Targeted gene-expression as a means of altering cell fates and generating dominant phenotypes. Development *118*, 401–415.

Brotz, T.M., and Borst, A. (1996). Cholinergic and GABAergic receptors on fly tangential cells and their role in visual motion detection. J. Neurophysiol. *76*, 1786–1799.

Burr, D., and Thompson, P. (2011). Motion psychophysics: 1985-2010. Vision Res. *51*, 1431–1456.

Cavanagh, P., and Mather, G. (1989). Motion: the long and short of it. Spat. Vis. *4*, 103–129.

Christiansen, F., Zube, C., Andlauer, T.F., Wichmann, C., Fouquet, W., Owald, D., Mertel, S., Leiss, F., Tavosanis, G., Luna, A.J., et al. (2011). Presynapses in Kenyon cell dendrites in the mushroom body calyx of *Drosophila*. J. Neurosci. *31*, 9696–9707.

Chubb, C., and Sperling, G. (1988). Drift-balanced random stimuli: a general basis for studying non-Fourier motion perception. J. Opt. Soc. Am. A *5*, 1986–2007.

Demb, J.B., Zaghloul, K., and Sterling, P. (2001). Cellular basis for the response to second-order motion cues in Y retinal ganglion cells. Neuron *32*, 711–721.

Fosque, B.F., Sun, Y., Dana, H., Yang, C.T., Ohyama, T., Tadross, M.R., Patel, R., Zlatic, M., Kim, D.S., Ahrens, M.B., et al. (2015). Neural circuits. Labeling of active neural circuits *in vivo* with designed calcium integrators. Science *347*, 755–760.

Götz, K.G. (1964). Optomoter studies of the visual system of several eye mutants of the fruit fly *Drosophila*. Kybernetik *2*, 77–92.

Götz, K.G., and Wenking, H. (1973). Visual control of locomotion in the walking fruitfly *Drosophila*. J. Comp. Physiol. *85*, 235–266.

Gordon, M.D., and Scott, K. (2009). Motor control in a *Drosophila* taste circuit. Neuron *61*, 373–384.

Groleau, M., Kang, J.I., Huppé-Gourgues, F., and Vaucher, E. (2015). Distribution and effects of the muscarinic receptor subtypes in the primary visual cortex. Front. Synaptic Neurosci. *7*, 10.

Hassenstein, B., and Reichardt, W. (1956). Systemtheoretische analyse der zeit, reihenfolgen und vorzeichenauswertung bei der bewegungsperzeption des russelkafers chlorophanus. Z. Naturforsch. B *11*, 513–524.

Heisenberg, M., and Wolf, R. (1984). Vision in *Drosophila*. Genetics of Microbehavior (Springer-Verlag Berlin Heidelberg).

Herrero, J.L., Roberts, M.J., Delicato, L.S., Gieselmann, M.A., Dayan, P., and Thiele, A. (2008). Acetylcholine contributes through muscarinic receptors to attentional modulation in V1. Nature *454*, 1110–1114.

Ito, K., Shinomiya, K., Ito, M., Armstrong, J.D., Boyan, G., Hartenstein, V., Harzsch, S., Heisenberg, M., Homberg, U., Jenett, A., et al. (2014). A systematic nomenclature for the insect brain. Neuron *81*, 755–765.

Kang, J.I., Huppé-Gourgues, F., and Vaucher, E. (2014). Boosting visual cortex function and plasticity with acetylcholine to enhance visual perception. Front. Syst. Neurosci. *8*, 172.

Katsov, A.Y., and Clandinin, T.R. (2008). Motion processing streams in *Drosophila* are behaviorally specialized. Neuron *59*, 322–335.

Keleş, M., and Frye, M.A. (2017). The eyes have it. Elife *6*, e24896.

Klinkenberg, I., and Blokland, A. (2010). The validity of scopolamine as a pharmacological model for cognitive impairment: a review of animal behavioral studies. Neurosci. Biobehav. Rev. *34*, 1307–1350.

Lee, Y.J., and Nordstrom, K. (2012). Higher-order motion sensitivity in fly visual circuits. Proc. Natl. Acad. Sci. U S A *109*, 8758–8763.

Leiss, F., Koper, E., Hein, I., Fouquet, W., Lindner, J., Sigrist, S., and Tavosanis, G. (2009). Characterization of dendritic spines in the *Drosophila* central nervous system. Dev. Neurobiol. *69*, 221–234.

Lima, S.Q., and Miesenböck, G. (2005). Remote control of behavior through genetically targeted photostimulation of neurons. Cell *121*, 141–152.

Lu, Z.L., and Sperling, G. (1995). The functional architecture of human visual motion perception. Vision Res. *35*, 2697–2722.

Mauss, A.S., Vlasits, A., Borst, A., and Feller, M. (2017). Visual circuits for direction selectivity. Annu. Rev. Neurosci. *40*, 211–230.

Nishida, S. (2011). Advancement of motion psychophysics: review 2001-2010. J. Vis. *11*, 11.

Orger, M.B., Smear, M.C., Anstis, S.M., and Baier, H. (2000). Perception of Fourier and non-Fourier motion by larval zebrafish. Nat. Neurosci. *3*, 1128–1133.

Qin, B., Humberg, T.H., Kim, A., Kim, H.S., Short, J., Diao, F., White, B.H., Sprecher, S.G., and Yuan, Q. (2019). Muscarinic acetylcholine receptor signaling generates OFF selectivity in a simple visual circuit. Nat. Commun. *10*, 4093.

Quenzer, T., and Zanker, J. (1991). Visual detection of paradoxical motion in flies. J. Comp. Physiol. A *169*, 331–340.

Rosenberg, A., and Issa, N.P. (2011). The Y cell visual pathway implements a demodulating nonlinearity. Neuron *71*, 348–361.

Rosenberg, A., Husson, T.R., and Issa, N.P. (2010). Subcortical representation of Non-Fourier image features. J. Neurosci. *30*, 1985–1993.

Schnell, B., Raghu, S.V., Nern, A., and Borst, A. (2012). Columnar cells necessary for motion responses of wide-field visual interneurons in *Drosophila*. J. Comp. Physiol. *198*, 389–395.

Sen, R., Wu, M., Branson, K., Robie, A., Rubin, G.M., and Dickson, B.J. (2017). Moonwalker

descending neurons mediate visually evoked retreat in *Drosophila*. Curr. Biol. *27*, 766–771.

Shearin, H.K., Quinn, C.D., Mackin, R.D., Macdonald, I.S., and Stowers, R.S. (2018). t-GRASP, a targeted GRASP for assessing neuronal connectivity. J. Neurosci. Methods *306*, 94–102.

Strauss, R., Schuster, S., and Götz, K.G. (1997). Processing of artificial visual feedback in the walking fruit fly *Drosophila melanogaster*. J. Exp. Biol. *200*, 1281–1296.

Sweeney, S.T., Broadie, K., Keane, J., Niemann, H., and O'Kane, C.J. (1995). Targeted expression of tetanus toxin light chain in *Drosophila* specifically eliminates synaptic transmission and causes behavioral defects. Neuron *14*, 341–351.

Takemura, S.Y., Karuppudurai, T., Ting, C.Y., Lu, Z., Lee, C.H., and Meinertzhagen, I.A. (2011). Cholinergic circuits integrate neighboring visual signals in a *Drosophila* motion detection pathway. Curr. Biol. *21*, 2077–2084.

Theobald, J.C., Duistermars, B.J., Ringach, D.L., and Frye, M.A. (2008). Flies see second-order motion. Curr. Biol. *18*, R464–R465.

Theobald, J.C., Shoemaker, P.A., Ringach, D.L., and Frye, M.A. (2010). Theta motion processing in fruit flies. Front. Behav. Neurosci. *4*, 35.

Vaina, L.M., and Cowey, A. (1996). Impairment of the perception of second order motion but not first order motion in a patient with unilateral focal brain damage. Proc. Biol. Sci. *263*, 1225–1232.

Vaina, L.M., Soloviev, S., Bienfang, D.C., and Cowey, A. (2000). A lesion of cortical area V2 selectively impairs the perception of the direction of first-order visual motion. Neuroreport *11*, 1039–1044.

Wolf, R., and Heisenberg, M. (1980). On the fine structure of yaw torque in visual flight orientation of *Drosophila melanogaster*. J. Comp. Physiol. *140*, 69–80.

Wu, M., Nern, A., Williamson, W.R., M orimoto, M.M., Reiser, M.B., Card, G.M., and Rubin, G.M. (2016). Visual projection neurons in the *Drosophila* lobula link feature detection to distinct behavioral programs. eLife *5*, e21022.

Zanker, J.M. (1990). Theta motion: a new psychophysical paradigm indicating two levels of visual motion perception. Naturwissenschaften *77*, 243–246.

Zhang, X., Liu, H., Lei, Z., Wu, Z., and Guo, A. (2012). Lobula-specific visual projection neurons are involved in perception of motion-defined second-order motion in *Drosophila*. J. Exp. Biol. *16*, 524–534.

Zhang, Y.Q., Rodesch, C.K., and Broadie, K. (2002). Living synaptic vesicle marker: synaptotagmin-GFP. Genesis *34*, 142–145.

iScience, Volume *23*

Supplemental Information

Differentiation of Theta Visual Motion from Fourier Motion Requires LC16 and R18C12 Neurons in *Drosophila*

Xiaoxiao Ji, Deliang Yuan, Hongying Wei, Yaxin Cheng, Xinwei Wang, Jihua Yang, Pengbo Hu, Julia Yvonne Gestrich, Li Liu, and Yan Zhu

Supplemental Figures

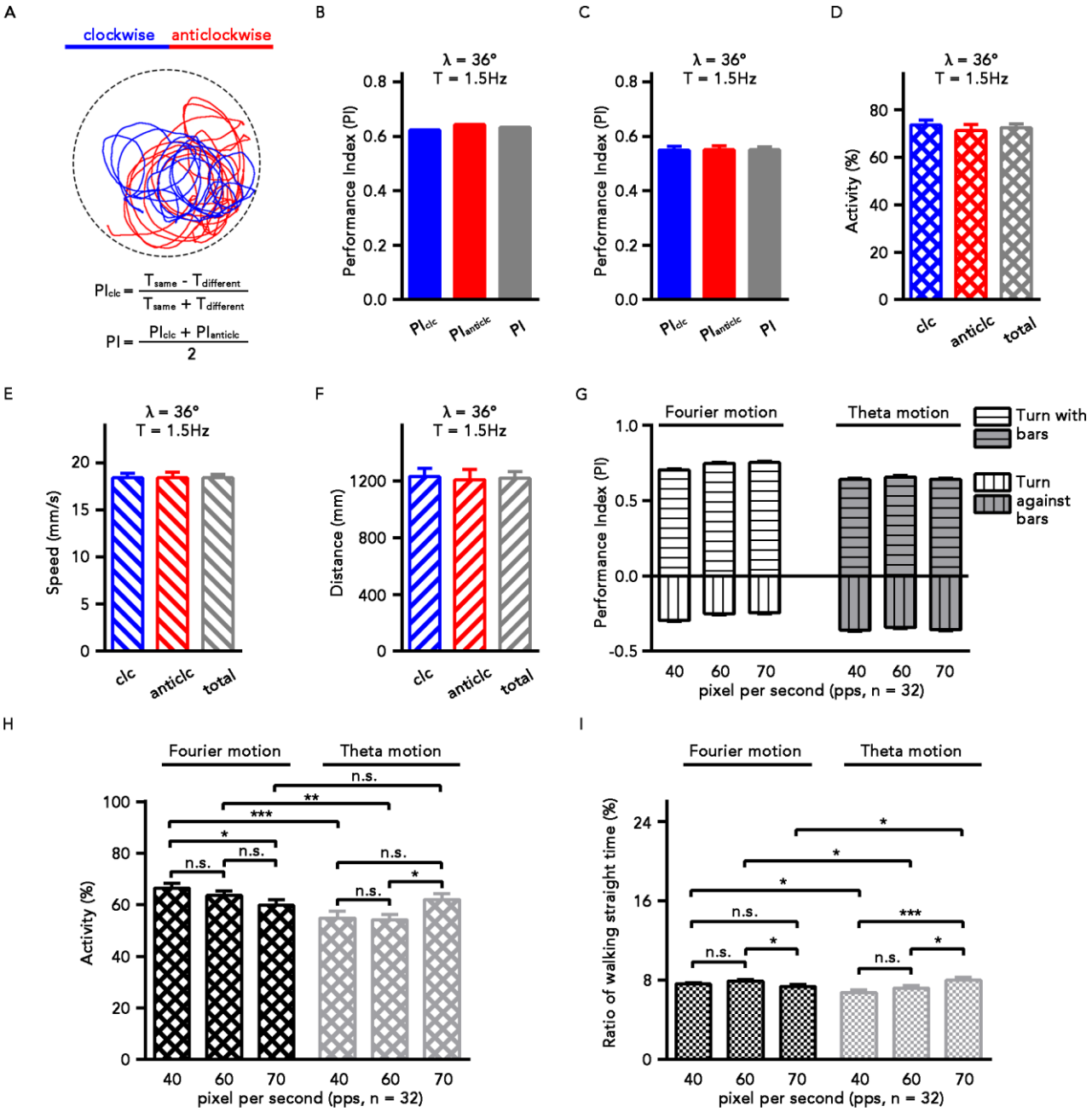

Figure S1. Calculating the Performance Index (PI) of motion tracking and other information through image analysis, Related to Figure 1. (A-F) WTCS flies were presented with a rotating black and white grating with wavelength of 36° at 1.5Hz. (A) The scheme of visual stimulations, corresponding walking traces, and PI calculation of a single wild-type fly. Blue indicates clockwise-rotated motion stimulus and corresponding trace, while red indicates anticlockwise stimulus and response. The black circle represents the border of the behavioral platform. (B) The PI_{clc}, $PI_{anticlc}$ and PI of the fly whose trajectories showed in (A). (C) Averaged PI_{clc}, $PI_{anticlc}$ and PI of 34 wild-type flies. (D) The flies showed similar averaged moving activities when presented with a visual motion rotated clockwise (n = 34), anticlockwise (n = 34), or both directions (total, n = 68). (E) The flies showed similar averaged moving speeds when presented with a visual motion rotated clockwise (n = 34), anticlockwise (n = 34) and both directions (total, n = 68). (F) The flies showed similar averaged moving distances when presented with a visual motion rotated clockwise (n = 34), anticlockwise (n = 34) and both directions (total, n = 68) of the flies. (G-I) WTCS flies were presented with visual

stimuli of various speed. The theta motion and Fourier motion stimuli were depicted in Figure 1C. (G) Analyzing the components of the responses in Figure 1D toward Fourier and theta motion stimuli of varying speeds. The positive values indicate the averaged proportion of time of a fly to rotate with the visual motion while the negative values indicate that against motion; the sum of each pair generated the corresponding PI value for that test condition (n = 32 each). (H) The averaged moving activities of WTCS flies presented with Fourier and theta motion stimuli at various speeds (n = 32 each). (I) Analyzing the proportion of time for WTCS flies to walk relative straight (the angle of turn < 0.5 degree) in the presence of Fourier and theta motion stimuli at various speeds (n = 32 each). Mann-Whitney test for (H) and (I). n.s., not significant, $p > 0.05$; *$p < 0.05$; **$p < 0.01$; ***$p < 0.001$.

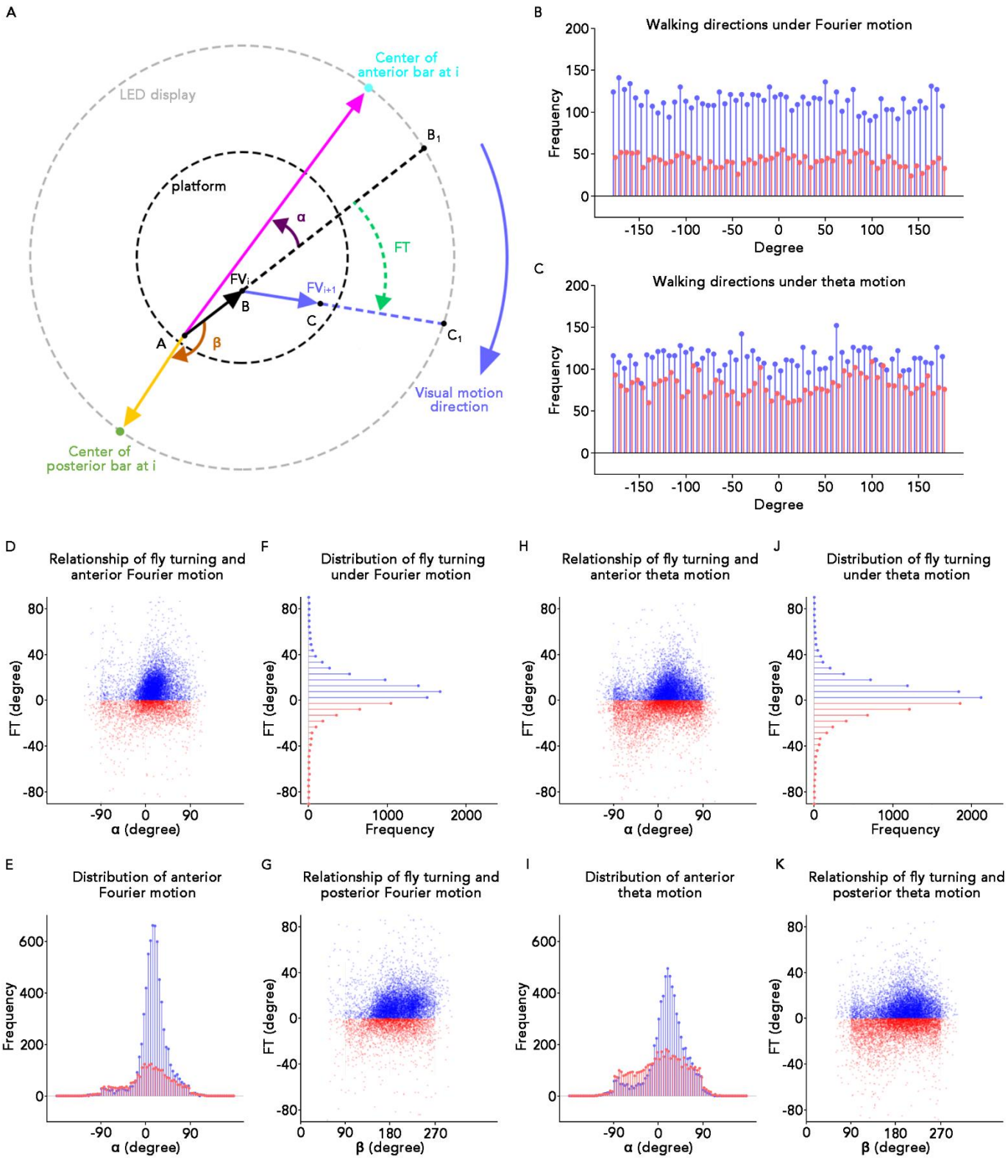
A
LED display
Center of anterior bar at i
B1
platform
α
FT
FVi
FVi+1
B
C
C1
A
β
Visual motion direction
Center of posterior bar at i
B
Walking directions under Fourier motion
Frequency
Degree
C
Walking directions under theta motion
Frequency
Degree
D
Relationship of fly turning and anterior Fourier motion
FT (degree)
α (degree)
F
Distribution of fly turning under Fourier motion
FT (degree)
Frequency
H
Relationship of fly turning and anterior theta motion
FT (degree)
α (degree)
J
Distribution of fly turning under theta motion
FT (degree)
Frequency
E
Distribution of anterior Fourier motion
Frequency
α (degree)
G
Relationship of fly turning and posterior Fourier motion
FT (degree)
β (degree)
I
Distribution of anterior theta motion
Frequency
α (degree)
K
Relationship of fly turning and posterior theta motion
FT (degree)
β (degree)

Figure S2. Analysis of spatial relationships between visual patterns and responding wild type flies, Related to Figure 1. (A) Schematic diagram showing the parameters used for correlation analysis. The fly was confined to walk within the platform, but not limited to the center of the platform. The visual stimuli were the same as those in Figure 1C. At any moment, the bar within the frontal view of the fly (its angle to the fly's heading direction is between ± 90 degrees) was defined as the anterior bar. In rare cases that both bars were in the frontal view or the posterior view, bar closer to the fly was defined as the anterior bar. The other bar was defined as the posterior bar. To quantify the causal relationship of rotating visual bars and the fly's movement, several parameters were defined from the perspective of the moving fly: FT, fly's turning angle ($\angle B_1BC_1$, also in figure 1B); α, the angle of the anterior bar to the fly's heading direction (a zero degree indicating the fly walked straight to this bar); β: the angle of the posterior bar to the fly; FV: fly's velocity (heading direction and distance). For every 0.1 s, these parameters were calculated, and "i" and "i+1" indicated two consecutive data points. Data points were split into two groups according to the fly's turning responses relative to the rotating visual bars: turning with the moving bars (blue) and turning against the moving bars (red) in (B) to (K). (B, C) Distributions of the heading angles of WTCS flies when presented with Fourier motion (B) or theta motion (C). (D-G) Analyzing the relationship between the turning response of WTCS flies and the angular position of Fourier motion. (D) A scatter plot showing the turning response vs. the angular position of the anterior rotating bars of Fourier motion. (E) Distribution of the angular positions in (D). (F) Distribution of the turning angles of the flies in (D). (G) A scatter plot showing the turning response vs. the angular position of the posterior bars of Fourier motion. (H-K) Analysis of the relationship between the turning response of WTCS flies and the angular position of the theta motion. (H) A scatter plot showing the turning response vs. the angular position of the anterior rotating bars of theta motion. (I) Distribution of the angular positions in (H). (J) Distribution of the turning angles of the flies in (H). (K) A scatter plot showing the turning response vs. the angular position of the posterior bars of theta motion. Each fly was tested with clockwise and anticlockwise motion stimuli at 60 pps. For anticlockwise motions, the signs of the turning and rotating angles were reversed, which meant that all the data points were normalized to clockwise motion. The number of flies: 12 for Fourier motion, and 16 for theta motion. The number of valid data points were 6812 (with motion) and 2535 (against motion) in (B) and (D)-(G); the number of valid data points were 6782 (with motion) and 4831(against motion) in (C) and (H)-(K). Certain data points were excluded from the analyses by the following criteria: 1) no fly was detected, or the parameters of detected flies were out of normal range in a video frame; 2) the calculated movements of flies between frames were out of standard range; 3) a fly moved less than 4 pixels (0.5 mm) between two consecutive time points (0.1 s).

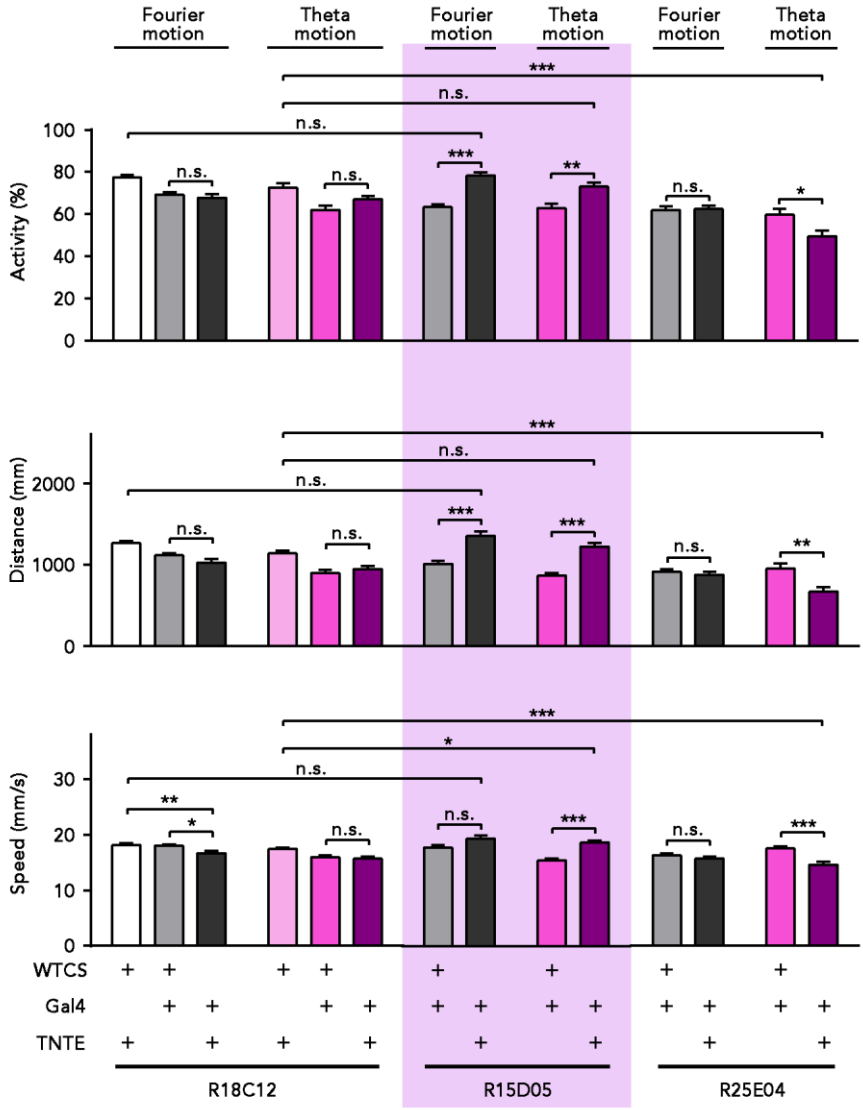

Figure S3. Comparison of moving activity, distance and speed of the R18C12>TNTE, R15D05>TNTE, R25E04>TNTE flies and their corresponding controls, Related to Figure 2. Flies were presented with Fourier motion and theta motion stimuli at 60 pps (n = 20~32; n.s., not significant, $p > 0.05$; *$p < 0.05$; **$p < 0.01$; ***$p < 0.001$; Mann-Whitney test).

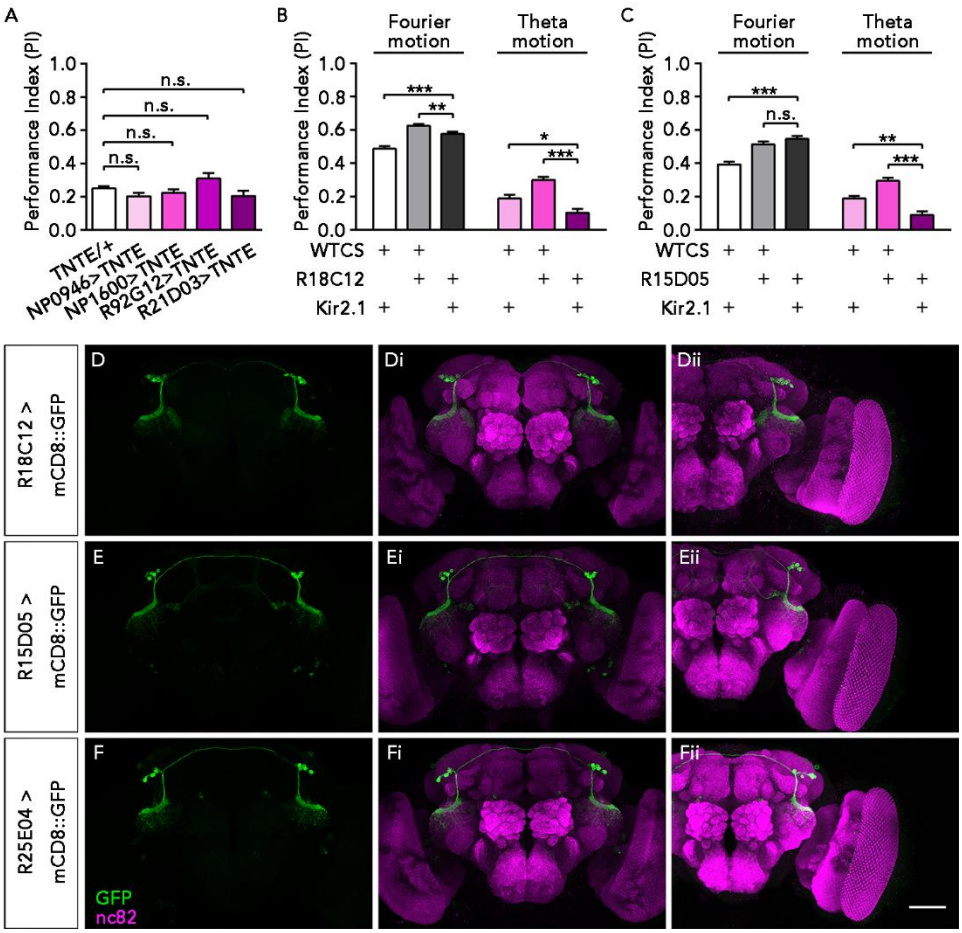

Figure S4. Comparison of the behavioral changes after silencing R18C12 and other neurons and the corresponding expression patterns, Related to Figure 2. (A) Blocking several other Gal4s labeled neurons had no influence on the theta motion perception in the flies (n = 20~32; n.s., not significant, $p > 0.05$; unpaired *t*-test). (B) The PI values of R18C12>Kir2.1 flies and genetic controls when presented with Fourier motion and theta motion stimuli at 60 pps (n = 30 each; *$p < 0.05$; **$p < 0.01$; ***$p < 0.001$; Mann-Whitney test). (C) The PI values of R15D05>Kir2.1 flies and genetic controls when presented with Fourier motion and theta motion stimuli at 60 pps (n = 20~40; n.s., not significant, $p > 0.05$; **$p <$ 0.01; ***$p < 0.001$; unpaired *t*-test). (D-Dii) Expression of mCD8::GFP under the control of R18C12-GAL4 in the central brain. (E-Eii) Expression of mCD8::GFP under the control of R15D05-GAL4 in the central brain. (F-Fii) Expression of mCD8::GFP under the control of R25E04-GAL4 in the central brain. GFP signals were not found in the optic lobes in all of these lines. Scale bar applied to all panels, 50 μm. Green, GFP signal; magenta, nc82 signal.

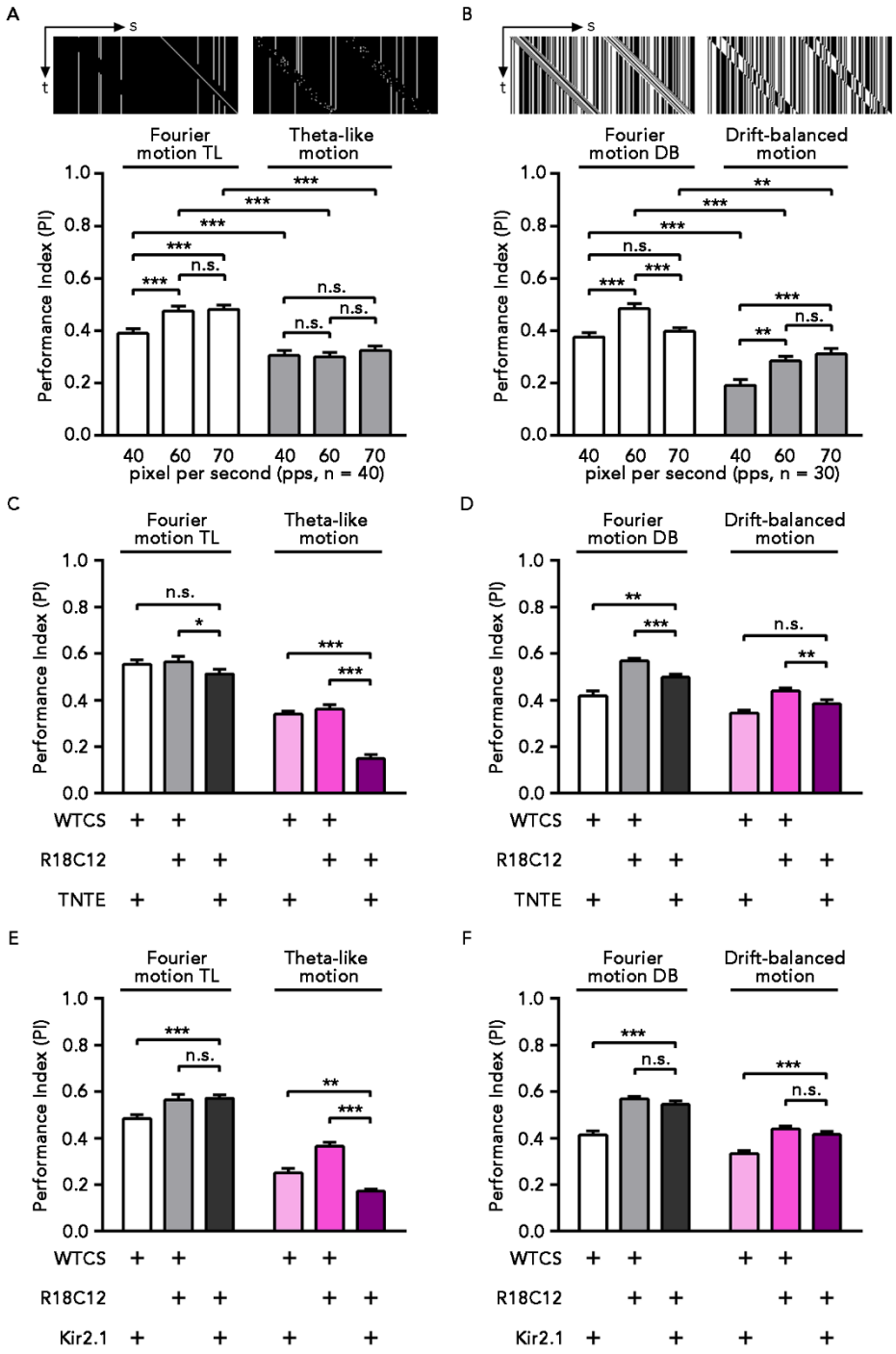

Figure S5. Comparison of visual responses between WTCS and the flies with silenced R18C12 neurons, Related to Figure 1 and 2. (A) The PI scores of WTCS flies when presented with theta-like motion and Fourier motion TL stimuli at various speeds (n = 40 each; n.s., not significant, $p > 0.05$; ***$p < 0.001$; Mann-Whitney test). Upper panels showed the space-time plots of theta-like motion and Fourier motion TL stimuli. (B) The PI scores of WTCS flies when presented with drift-balanced motion and Fourier motion DB stimuli at various speeds (n = 30 each; n.s., not significant, $p > 0.05$; **$p < 0.01$; ***$p < 0.001$; Mann-Whitney test). Upper panels showed the space-time plots of drift-balanced motion and Fourier motion DB stimuli. (C) The PI values of R18C12>TNTE flies and their genetic controls when presented with theta-like motion and Fourier motion TL stimuli at 60 pps (n = 30 each; n.s., not significant, $p > 0.05$; *$p < 0.05$; ***$p < 0.001$; Mann-Whitney test). (D) The PI values of R18C12>TNTE flies and their genetic controls when presented with drift-balanced motion and Fourier motion DB stimuli at 60 pps (n = 32 each; n.s., not significant, $p > 0.05$; **$p < 0.01$; ***$p < 0.001$; Mann-Whitney test). (E) The PI values of R18C12>Kir2.1 flies and their genetic

controls when presented with theta-like motion and Fourier motion TL stimuli at 60 pps (n = 32 each; n.s., not significant, $p > 0.05$; **$p < 0.01$; ***$p < 0.001$; Mann-Whitney test). (F) The PI values of R18C12>Kir2.1 flies and their genetic controls when presented with drift-balanced motion and Fourier motion DB stimuli at 60 pps (n = 30~32 each; n.s., not significant, $p > 0.05$; ***$p < 0.001$; Mann-Whitney test).

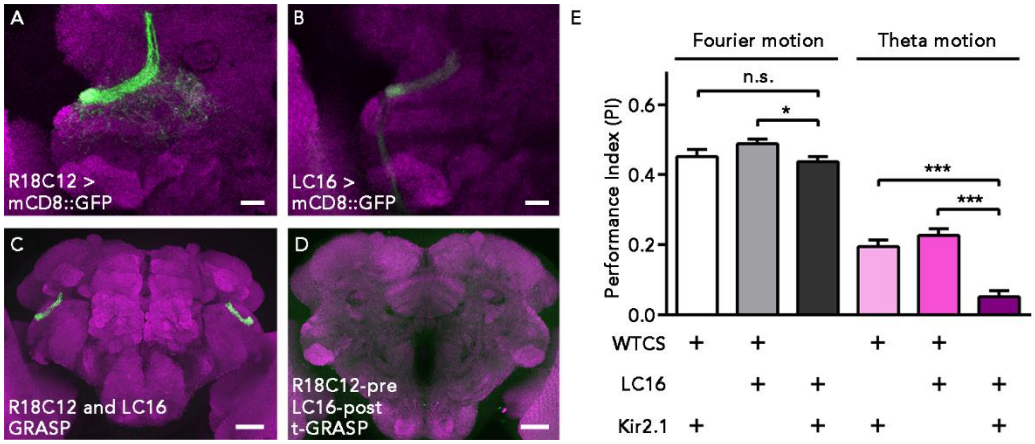

Figure S6. LC16 connected with R18C12 neurons and was involved in theta motion perception, Related to Figure 4. (A) Expression of mCD8::GFP under the control of R18C12-GAL4 in VLP region. (B) Expression of mCD8::GFP under the control of LC16-GAL4 (OL0092C) in VLP region. (C) The GRASP signal (green) reconstituted by GFP11 under the control of R18C12-LexA and GFP1-10 under the control of LC16-Gal4. (D) No t-GRASP signal was observed in flies with pre-t-GRASP (GFP11) under the control of R18C12-LexA and post-t-GRASP (GFP1-10) under the control of LC16-Gal4. Nc82 served as counterstaining (magenta). Scale bar applied to (A-B), 10 μm and (C-D), 30 μm. (E) The PIs of LC16>Kir2.1 flies and their genetic control flies when presented with Fourier motion and theta motion stimuli at 60 pps (n = 20 each; n.s., not significant, $p > 0.05$; *$p < 0.05$; ***$p < 0.001$; unpaired *t*-test).

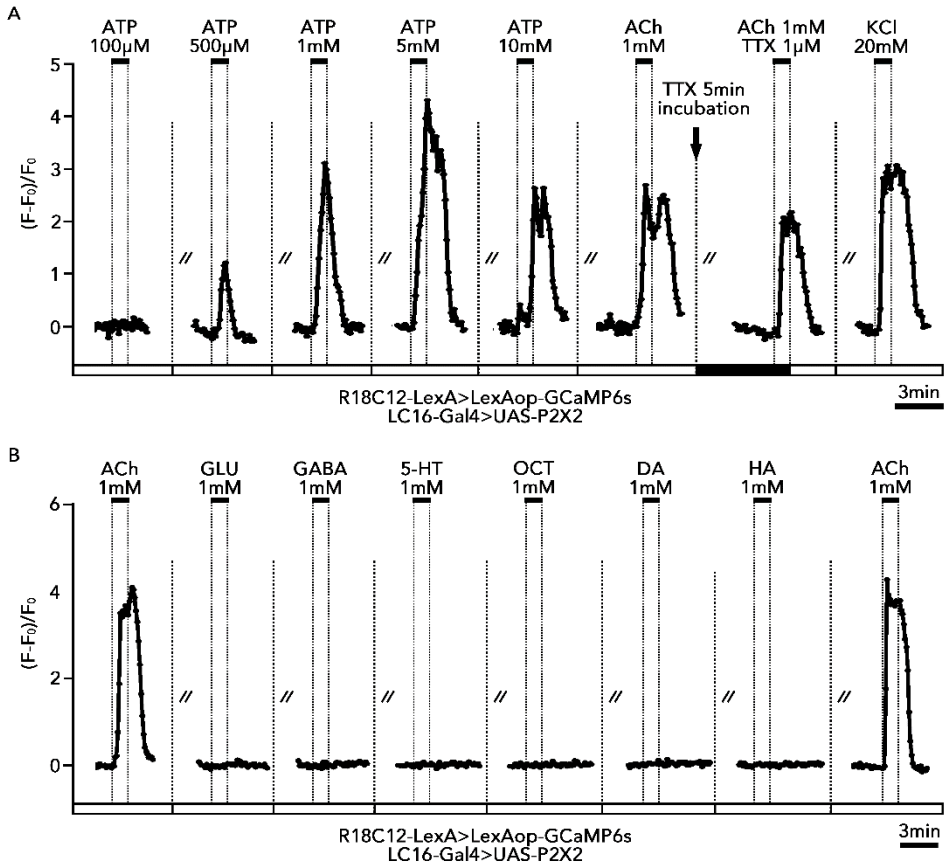

Figure S7. Changes in intracellular calcium levels of R18C12 neurons in response to ATP and neurotransmitters, Related to Figure 4. (A) $\Delta F/F$ traces showing the calcium response of a R18C12 neuron to increasing concentrations of ATP. The intracellular calcium level increased immediately after ATP applications. At higher concentrations of ATP, intracellular calcium level first increased but decayed afterward. The solid bars on top indicate the durations of each ATP application. Calcium responses in R18C12 neurons were not significantly blocked by 1 μM TTX application (n = 6). (B) The R18C12 neurons were only activated by ACh treatment. Representative $\Delta F/F$ traces of calcium responses in R18C12 neurons were shown here. The calcium level of the R18C12 neurons increased after 1 mM ACh treatment, whereas there were no responses after adding 1 mM GABA, glutamate, dopamine, octopamine, serotonin or histamine (n = 6).

Transparent Methods

Fly stocks and genetics

Flies were raised on a standard medium of corn meal and molasses (Guo et al., 1996) in a 12 h : 12 h light/dark cycle at 60 % relative humidity.

The following lines were used for experiments: Wild-type Canton S (WTCS), UAS-TNTE (Sweeney et al., 1995), UAS-Kir2.1 (Baines et al., 2001), UAS-mCD8::GFP (Lee and Luo, 1999), UAS-syt::GFP (Zhang et al., 2002), UAS-Dα7::GFP (Leiss et al., 2009), UAS-GFP.nls (Shiga et al., 1996), R18C12-Gal4, R18C12-LexA, R15D05-Gal4, R25E04-Gal4, R92G12-Gal4, R21D03-Gal4 (Jenett et al., 2012), UAS-CaMPARI (Fosque et al., 2015), OL0092C (LC16-Gal4, Wu et al., 2016), UAS-CD4::GFP1–10,LexAop-CD4::GPF11 (Gordon and Scott, 2009), UAS-post-t-GRASP,LexAop2-pre-t-GRASP, LexAop2-post-t-GRASP,UAS-pre-t-GRASP (Shearin et al., 2018), LexAop-GCaMP6s (Strother et al., 2017), UAS-P2X2 (Lima and Miesenböck, 2005), NP0946-Gal4, NP1600-Gal4 (*Drosophila* Genetic Resource Center at the Kyoto Institute of Technology).

Behavioral paradigm

We used a color LED-based system to test the visual motion perception of freely walking flies (Zhou et al., 2012). A cylindrical LED screen containing 200 (column) × 64 (row) pixels displayed different stimuli under the control of LED Studio software (Shenzhen Sinorad Medical Electronics, Shenzhen, China) on the connected computer. The screen was 300 mm in diameter and 330 mm in height. The refresh rate of the LED screen was 70 Hz, which was identical to the refresh rate of the display of the controlling computer. The refresh speeds were verified by a high-speed camera. The LED screen constituted the wall of the setup, and the computer and its display were visually separated from the LED cylinder and the flies' view.

At the bottom center of the set-up, there was a circular platform with a diameter of 100 mm for a wing-clipped fly to walk on. A water-filled moat was located between the platform and the LED screen to prevent the fly from escaping. A camera (WV-BP330, Panasonic System Networks) suspended 540 mm above the platform was used to record the images of the platform at a rate of 12 frames per second.

We tested 3–6 day-old flies in the behavioral experiments. Male and female flies were used alternately. Before the tests, the wings of flies were clipped to one-third of their normal length under CO_2 anesthesia, and flies were allowed to recover for at least 24 h before behavioral experiments. The flies were tested individually for visual perception. A fly was permitted to walk freely on the round platform at the center of the apparatus during the test. The fly was presented with a visual stimulus that was first rotated clockwise for 90 s, then rotated counter-clockwise for another 90 s.

The position and trajectory of the fly in each frame were calculated by Limelight software (Coulbourn Instruments, Whitehall, PA, USA). From this information, the performance index (PI) was calculated with custom scripts in MATLAB (Mathworks, Natick, MA).

Performance Index

A schematic diagram outlining the performance index was shown in Figure 1B. To simplify the quantification, only the direction of the fly's turning was considered. Assuming a fly walks from A to B then to C in two sequential frames, projecting its trajectory on the visual display forms point B_1 and C_1, the direction from B_1 to C_1 represents the turning response of the fly to the visual motion. If the fly turns clockwise as the visual motion, it exhibits a positive response to the stimulus (turning with the motion). If the fly turns against the visual motion (from A to B, then to C', corresponding projection points of B_1 and C_1'), it has a negative response (turning against the motion).

To summarize the responses of the fly over all time points, we calculated T_{same}, the total duration for which the fly tracked the visual motion, and $T_{different}$, the total duration for which the fly walked against the visual motion. When there was no apparent movement between frames, the time points would be excluded. The Performance Index for anticlockwise visual motion, $PI_{anticlc}$, was defined as: $(T_{same} - T_{different})/(T_{same}+T_{different})$. Similarly, for clockwise motion,

the Performance Index, PI_{clc}, was obtained. The overall performance of a single fly was quantified as the average of PI_{clc} and $PI_{anticlc}$ (Figure S1A). This PI indicates the motion tracking ability of the free walking fly. If the tested fly tracks the visual motion stimulus most of the time, then its PI would be significantly higher than zero ($0 < PI \leq 1$); if the fly does not track the stimulus at all, the PI would be close to zero ($PI = 0$); if the fly turns against the visual motion stimulus for most of the test period, the PI value would be negative ($-1 \leq PI < 0$).

In addition, the locomotion activity of a fly was quantified by calculating the proportion of walking time during the test period. The total moving distance of a fly was the sum of all walking distances during the test. The average speed of a fly was the result of the total moving distance divided by the total walking time.

Visual stimuli

The visual stimuli presented on the panoramic LED screen contained black and white dots or stripes, generating a theoretic contrast of 100 %.

To investigate the higher-order motion perception in free-walking flies, we used three pairs of stimuli, each of which included a type of higher-order motion and the corresponding first-order motion. They were **theta motion** and **Fourier motion**, **theta-like motion** and **Fourier motion TL**, and **drift-balanced motion** and **Fourier motion DB** as described below. Each stimulus contained two bars (16-pixel width, 180° apart) moving horizontally. The rotation speeds of the bars in the higher-order motion and corresponding first-order motion were equal, for direct comparisons. At the center of the platform, the mean luminance values of theta, theta-like, drift-balanced motion were 162 lux, 21.5 lux, and 225 lux, respectively.

Theta motion and **Fourier motion** As the primary visual stimuli tested, theta motion and Fourier motion contained 40 % white and 60 % black random dots (Video S1). A theta motion contained both first- and higher-order motion cues, but these cues oriented in opposite horizontal directions. In other words, when two higher-order motion bars (moving windows) moved rightwards, the first-order moving dots (dots inside the bars) would move leftwards; both move at the same relative speed to the background. Theta motion has often been used in previous investigations of higher-order motion (Theobald et al., 2008; Theobald et al., 2010; Zhang et al., 2012).

The corresponding Fourier motion, as first-order motion, contained the same background as the theta motion stimuli (40 % white and 60 % black random dots). When the first-order bars were moving, the dots inside the bar also moved in the same direction at the same speed as the moving bars. In other words, the dots were static relative to the bars and appeared to be moving with the bars.

Theta-like motion and **Fourier motion TL** The pair contained 5 % white dots and 95 % black random dots (Video S2). Inside the theta-like moving bars, the internal dots moved perpendicular to the bar movement. Thus, the dots inside the horizontally moving bars moved up or down randomly, without generating coherent first-order cues along the horizontal directions. The theta and theta-like motion were also called motion-defined higher-order motion (MDSM).

Fourier motion TL was first-order motion with the same background as the corresponding theta-like motion. Fourier motion TL was similar to Fourier motion above, but with lower dot density ($d = 0.05$, rather than 0.4 in Fourier motion). In Fourier motion TL, the dots inside the bars were static and moved along with the bars.

Drift-balanced motion and **Fourier motion DB** contained 50 % white and 50 % black random stripes (Video S3). In drift-balanced motion, the higher-order moving bars inverted the luminance of the background under them. Thus, as the bars moved through the background, the pixels inside the bars inverted their luminance, either from white to black or from black to white, depending on the original background in the same position.

Fourier motion DB was first-order motion with the same background as the corresponding drift-balanced motion. Fourier motion DB also had two bars consisting of 50 % white and 50 % black random stripes. The pixel patterns inside the bar did not change while the bar was moving. The motion of first-order moving bars with a fixed pattern formed coherent space-

time correlations in luminance.

Except for the experiments on velocity parameters, the speed of visual motions used in behavioral tests was 60 pps, meaning that the two bars moved horizontally 60 pixels per second, equivalent to 3.33 second per cycle. In velocity tests, the motion speeds were 40 pps, 60 pps and 70 pps (Figure 1D, S1G-I, S5A and S5B). Every pixel was equivalent to a visual angle of approximately 1.8° from the center of the platform. When the flies walked freely on the platform, the visual angle of one pixel varied, ranging from 1.35° (minimum) to 2.7° (maximum).

Immunohistochemistry and imaging

Adult flies (3–6 days old) were first immobilized by placing the container on ice, then pinned on a sylgard-coated preparation chamber filled with cold phosphate-buffered saline (PBS). The head cuticles, eyes, proboscis, and trachea were carefully removed with fine forceps. The brain samples were fixed in freshly prepared paraformaldehyde (4 % in PBS) for 2 h on ice, then washed for 3 × 15 min in PBT (PBS with 0.5 % Triton X-100), followed by incubation in PNT (10 % normal goat serum in PBT) for 1 h at room temperature. Next, samples were incubated with primary antibodies diluted in PNT overnight at 4 °C. Samples were then washed in PBT for 3 × 15 min at room temperature and subsequently incubated overnight with secondary antibodies diluted by PNT at 4 °C. After being rinsed in PBT for 3 × 15 min, samples were mounted in Vectashield Fluorescent Mounting Media (Vector Laboratories, Burlingame, USA) and observed.

For transmitter related immunostaining experiments, 1 day old adult female flies were used. The brain samples were fixed in freshly prepared paraformaldehyde (4 % in PBS) overnight at 4 °C, then washed for 4 × 15 min in PBT (PBS with 0.5 % Triton X-100), followed by incubation in PNT (10 % normal goat serum in PBT) for 3 h at room temperature. Next, samples were incubated with primary antibodies diluted in PNT for 72 h at 4 °C. Samples were then washed in PBS three times for 8 h and then incubated for 24 h in secondary antibodies at 4 °C. After being rinsed in PBS overnight, samples were mounted and observed.

The following antibodies were used with indicated dilutions: mouse nc82 antibody (1:200) and mouse anti-ChAT4B1 antibody (1:10), both from Developmental Studies Hybridoma Bank, University of Iowa, USA; FITC-conjugated rabbit anti-GFP antibodies (1:400, abcam #ab66180), Cy3-conjugated goat anti-mouse antibodies (1:400 for common staining experiments and 1:100 for transmitter related staining experiments, Jackson ImmunoResearch Laboratories #115-165-062).

Brains were scanned with a confocal microscope (Leica TCS SP5 or SP8). Stacks of optical sections at 2 μm spacing were collected at a resolution of 1024 × 1024 pixels. The images were then processed with ImageJ (National Institutes of Health, rsbweb.nih.gov/ij/).

Electrophysiology

Patch-clamp recordings of neurons in the brain of fruit flies were carried out *in vivo*, with the following protocol. One- to two-day-old female flies were anesthetized with ice and fixed individually in a recording chamber (Figure 3A). The head was kept steady in a recording holder. A small region of the head capsule was removed, and extracellular Ringer's solution (101 mM NaCl, 3 mM KCl, 4 mM $MgCl_2$, 1 mM $CaCl_2$, 5 mM glucose, 20.7 mM $NaHCO_3$, 1.25 mM NaH_2PO_4, pH 7.2, osmolarity of 265 mmol/kg) was supplied (Yang et al., 2011). The perineural sheath was gently removed. The recording chamber was continuously perfused with Ringer solution bubbled with 95 % O_2 and 5 % CO_2 (2 mL/min). The R18C12 neurons were identified by their fluorescence and morphology under a 40x objective, and upper neurons were removed with borosilicate glass capillaries (2 MΩ, GCF150-7.5, Harvard Apparatus, USA) prepared on a Flaming/Brown P-87 micropipette puller (Sutter Instruments, Novato, USA) to get access to the cells. Current-clamp recordings were performed using borosilicate glass capillaries (B15024F, Vitalsense Scientific Instruments Co., Ltd.) and filled with internal solution (102 mM K-gluconate, 0.085 mM $CaCl_2$, 0.94 mM EGTA, 8.5 mM HEPES, 1.7 mM $MgCl_2$, 17 mM NaCl, adjusted to 235 mOsm, pH 7.2). All electrophysiological recordings were carried out using Nikon upright microscope (NI-FLT6) equipped with a mercury lamp (OSRAM) and a GFP filter (BP 450–480). Signals were acquired with an Axon-700B multiclamp amplifier, digitized at 25 kHz and filtered at 2 kHz using a Digidata 1550

(Axon Instruments, California, USA) converter. Data were analyzed using Clampex 9.0 software (Molecular Devices). The maximum action potential frequencies were calculated by Spikes2.0 software (Cambridge Electronic Design Limited, Cambridge, ENGLAND).

Visual stimuli were presented through a customized, light-emitting diode (LED) arena composed of 96 (column) × 48 (row) pixels. The arena was mounted in front of the immobilized fly. The LED arena provided one eye with a 54° (vertical) by 127° (horizontal) visual field (Figure 3A). The shortest distance between the arena and fly was 11.5cm. A customized controller panel, controlled by scripts of MATLAB, was used to display visual motion stimuli, Fourier and theta motion, on the LED arena (Figure 1C).

CaMPARI photo-conversion experiment

An adult fly (3–6 days old) was fixed on top of a micropipette tip (200 µl, with a widened opening), with its head protruding from the tip (Shiraiwa and Carlson, 2007). The micropipette tip was placed in front of two symmetrical square LED screens (32 × 32 pixels), which formed a right angle. When presenting visual motions to the fly, a 405 nm laser was focused on the region between the fly's compound eyes on the brain through the gap between the two screens. The diameter of the light spot was less than 0.3 mm. 1 Hz pulses of 5 mW/mm^2 photo-conversion (PC) light were used for PC to minimize photo-damage to the animal. The PC light lasted 90 s, while the visual stimulus was presented on the screen.

In the experimental group, the visual stimuli provided to the flies contained two 8-pixel-wide bars, which moved at 108 °/s (this is the same speed as the stimuli presented in the free walking paradigm). In the control group, flies were presented with a static random dots background, while all other parameters, including photo-conversion, were identical. Experimental flies and control flies were treated alternately.

After the treatment, flies were dissected in calcium-free EGTA-containing extracellular saline (103 mM NaCl, 3 mM KCl, 1 mM NaH_2PO_4, 4 mM $MgCl_2$, 10 mM D-(+)-trehalose dehydrate, 10 mM D-(+)-glucose, 5 mM N-tris(hydroxymethyl) methyl-2-aminoethane sulfonic acid, 26 mM $NaHCO_3$, and 5 mM EGTA, pH 7.4) and imaged immediately with a confocal microscope (Leica TCS SP8) using a 20× objective lens. We used 488 nm and 552 nm lasers for imaging.

Images were analyzed with a custom program written in MATLAB. 2D regions of interest (ROIs) were manually determined to include the candidate neurons and exclude surrounding tissues. The fluorescence values within ROIs in each color channel (green and red) were calculated and thresholded to restrict the candidate neurons further. Finally, the average red and green fluorescence of the entire image stack were obtained, and the corresponding red/green ratio of the candidate neurons was calculated. The relative signal ratios of the experimental group were defined as the division of the red/green ratios of the experimental group with those of the control group. The relative signal ratios of the control group were defined as the red/green ratios of the control group divided by the average red/green ratios of the control group.

Calcium Imaging with ATP activation

Two- to four-day-old female flies were dissected in *Drosophila* adult extracellular Ringer's solution. Subsequently, each dissected brain was enzymatically digested (protease IV 1 mg/ml), then secured on a brain holder coated with poly-lysine (0.2 mg/ml) at the bottom of the perfusion chamber, anterior side up. The Ringer solution circulated via a pump at a speed of 2 mL/min and continuously superfused the neurons throughout the imaging experiment. First, baseline fluorescence was acquired for 2 min. For P2X2 experiments, we bath applied 1 mM ATP (Sigma Aldrich) for 60 s into the chamber (Zhou et al., 2019). After 2 min of stimulus presentation, the brain was superfused until the calcium fluorescence restored to the basal level. In the vehicle control group, Ringer's solution was applied for 60 s. For a viability-test on the neurons in the field, Ringer's solution containing 20 mM KCl was used to stimulate the living neurons, whose fluorescence increased in response to extracellular KCl.

In order to survey neurotransmitters to R18C12 neurons, the neurotransmitters acetylcholine, GABA, glutamate, dopamine, octopamine, serotonin, histamine and 20 mM KCl (Sigma Aldrich) were successively bath applied for 60 s each at a concentration of 1 mM. To analyze

the ATP responses, we successively bath applied the two drugs: Mecamylamine (MCA, 100 μM, blocks nicotinic acetylcholine receptors, nAChRs) (Huang et al., 2010) and Scopolamine (100 μM, Scop, blocks metabotropic acetylcholine receptors, mAChRs, Sigma Aldrich) (Gorczyca et al., 1991). Brains were first incubated with each antagonist for 5 min before ATP was bath applied, then the combined effect of each antagonist and ATP was examined.

Changes in calcium-induced fluorescence of GCaMP6s expressing cells were monitored using a Leica TCS SP8 confocal microscope with a 40× water-immersion objective. Images were acquired at a resolution of 512 × 256 pixels. Raw confocal images were processed in Amira (Thermo Fisher Scientific) and ImageJ. First, the image series were imported into Amira and aligned by shifting the images to maximize the correlation to a reference image. For analysis, the regions of interest (ROIs) containing GCaMP6s expressing cell bodies were identified individually by using ImageJ. The average fluorescence intensity within each ROI was calculated for each frame to create a response trace as a function of time. The fluorescence change was normalized by subtracting the background ($\Delta F/F = [F(t) - F_0(t)]/F_0$).

Statistics

Data analysis was performed in GraphPad Prism 6. The one-sample *t*-test was used to compare the PI with zero, which is the theoretical chance level. When evaluating the difference between two groups in behavioral experiments, the unpaired *t*-test was performed if all data in one figure panel showed normal distribution (determined by D'Agostino and Pearson omnibus normality test), otherwise Mann-Whitney test was performed. For electrophysiological, CaMPARI and calcium imaging, paired *t*-test was used to compare normally distributed two groups, while the Wilcoxon matched-pairs signed-rank test or Kolmogorov-Smirnov test was used to compare two groups of non-normal distribution. The significance levels of the statistical tests were set as $*p < 0.05$, $**p < 0.01$, $***p < 0.001$; n.s., not significant, $p > 0.05$. Error bars in the figures represent the standard error of the mean (SEM).

Supplemental References

Gorczyca, M.G., Budnik, V., White, K., and Wu, C.F. (1991). Dual muscarinic and nicotinic action on a motor program in *Drosophila*. J. Neurobiol. *22*, 391-404.

Guo, A., Liu, L., Xia, S.Z., Feng, C.H., Wolf, R., and Heisenberg, M. (1996). Conditioned visual flight orientation in *Drosophila*: dependence on age, practice, and diet. Learn. Mem. *3*, 49-59.

Huang, J., Zhang, W., Qiao, W., Hu, A., and Wang, Z. (2010). Functional connectivity and selective odor responses of excitatory local interneurons in *Drosophila* antennal lobe. Neuron *67*, 1021-1033.

Jenett, A., Rubin, G.M., Ngo, T.T., Shepherd, D., Murphy, C., Dionne, H., Pfeiffer, B.D., Cavallaro, A., Hall, D., Jeter, J., et al. (2012). A GAL4-driver line resource for *Drosophila* neurobiology. Cell Rep. *2*, 991-1001.

Lee, T., and Luo, L. (1999). Mosaic analysis with a repressible cell marker for studies of gene function in neuronal morphogenesis. Neuron *22*, 451-461.

Shiga, Y., Tanaka-Matakatsu, M., and Hayashi, S. (1996). A nuclear GFP/ beta-galactosidase fusion protein as a marker for morphogenesis in living *Drosophila*. Dev. Growth Differ. *38*, 99-106.

Shiraiwa, T., and Carlson, J.R. (2007). Proboscis extension response (PER) assay in *Drosophila*. J. Vis. Exp. *193*.

Strother, J.A., Wu, S.T., Wong, A.M., Nern, A., Rogers, E.M., Le, J.Q., Rubin, G.M., and Reiser, M.B. (2017). The emergence of directional selectivity in the visual motion pathway of *Drosophila*. Neuron *94*, 168-182. e10.

Yang, Y., Yan, Y., Zou, X., Zhang, C., Zhang, H., Xu, Y., Wang, X., Janos, P., Yang, Z., and Gu, H. (2011). Static magnetic field modulates rhythmic activities of a cluster of large local interneurons in *Drosophila* antennal lobe. J. Neurophysiol. *106*, 2127-2135.

Zhou, M., Chen, N., Tian, J., Zeng, J., Zhang, Y., Zhang, X., Guo, J., Sun, J., Li, Y., Guo, A., et al. (2019). Suppression of GABAergic neurons through D2-like receptor secures efficient conditioning in *Drosophila* aversive olfactory learning. Proc. Natl. Acad. Sci. U. S. A. *116*, 5118-5125.

Zhou, Y., Ji, X., Gong, H., Gong, Z., and Liu, L. (2012). Edge detection depends on achromatic channel in *Drosophila melanogaster*. J. Exp. Biol. *215*, 3478-3487.